frontiers in Earth Science

ORIGINAL RESEARCH
published: 01 April 2021
doi: 10.3389/feart.2021.648122

The Metallogeny of the Lubei Ni–Cu–Co Sulfide Deposit in Eastern Tianshan, NW China: Insights From Petrology and Sr–Nd–Hf Isotopes

Ping Li[1,2,3], Ting Liang[1]*, Yonggang Feng[1], Tongyang Zhao[2], Jiangtao Tian[2], Dahai Li[2], Jian Li[4], Gang Chen[2,3] and Changzhi Wu[1]*

[1] College of Earth Science and Resources, Chang'an University, Xi'an, China, [2] Xinjiang Bureau of Geological Mineral Exploration and Development, Urumqi, China, [3] Xinjiang Bureau of Geology and Mineral Resources, Urumqi, China, [4] Xinjiang Experimental Institute of Mineral Resources, Urumqi, China

OPEN ACCESS

Edited by:
Ryan Mathur,
Juniata College, United States

Reviewed by:
Yu-Feng Deng,
Hefei University of Technology, China
Rui Wang,
China University of Geosciences, China

***Correspondence:**
Ting Liang
liangt@chd.edu.cn
Ping Li
liping3731@163.com

Specialty section:
This article was submitted to Economic Geology, a section of the journal Frontiers in Earth Science

Received: *31 December 2020*
Accepted: *10 March 2021*
Published: *01 April 2021*

Citation:
Li P, Liang T, Feng Y, Zhao T, Tian J, Li D, Li J, Chen G and Wu C (2021) The Metallogeny of the Lubei Ni–Cu–Co Sulfide Deposit in Eastern Tianshan, NW China: Insights From Petrology and Sr–Nd–Hf Isotopes. Front. Earth Sci. 9:648122. doi: 10.3389/feart.2021.648122

The Lubei Ni–Cu–Co deposit situated in western segment of the Huangshan-Jing'erquan mafic–ultramafic rock belt in eastern Tianshan of the Central Asian Orogenic Belt (CAOB). The estimated reserve is approximately 9.11 million tons of ore resources with average grades of 0.82 wt% Ni, 0.52 wt% Cu, and 0.03 wt% Co. The Lubei intrusion is mainly composed of gabbro (phase I), peridotite (phase II), pyroxene peridotite (phase III), olivine pyroxenite (phase IV), and diorite (phase V), which intruded into the early Carboniferous tuffaceous clastic rocks. Zircon Laser Ablation–Inductively Coupled Plasma–Mass Spectrometry (LA–ICP–MS) U–Pb age of the diorite (phase V) from the edge of the intrusion is interpreted as the top-limit metallogenic age, which is consistent with the formation ages of the Huangshan and Xiangshan Ni–Cu deposits in eastern Tianshan. The roughly parallel rare earth element (REE) curves of the Lubei intrusion indicate the magma originated from a homologous source. The slightly enriched large ion lithophile elements (LILE) are compared to high field strength elements (HFSE) with negative Nb and Ta anomalies show that the Lubei intrusion has arc-affiliate geochemical characteristics. The Sr–Nd–Hf isotopes show that the magma was derived from depleted lithospheric mantle, while suffering 4–10% lower crustal contamination with slight contamination of the upper crust. Based on a comprehensive conservation of regional geological, geochemical, and geochronological evidence, the primary magma of the Lubei intrusion was identified that it was derived from the partial melting of metasomatized lithospheric mantle previously modified by subduction events. The Lubei nickel–copper–cobalt sulfide deposit was formed after the primary magma experienced fractional crystallization, crustal contamination, and sulfide segregation in a post-collisional extensional geodynamic setting after the closure of the Kanggur ocean basin in the early Permian.

Keywords: Sr–Nd–Hf isotopes, eastern Tianshan (NW China), metallogenic mechanism, Ni–Cu sulfide deposit, Lubei

INTRODUCTION

Most world-class magmatic Ni–Cu–PGE sulfide deposits were formed at cratons or at the margins in association with intraplate magmatism (Naldrett, 1999). Thus, the magmatic evolution and mineralization processes of magmatic Ni–Cu deposits within cratons have been well documented (Barnes and Lightfoot, 2005; Naldrett, 2009; Begg et al., 2010). However, relatively small magmatic sulfide deposits formed in orogenic belts have not been well studied and resulted in debates on their sulfide mineralization and magmatic conduit systems (Gao et al., 2012, 2013; Su et al., 2013b; Zhao et al., 2015; Deng et al., 2021).

The Central Asian Orogenic Belt (CAOB) is a typical accretionary orogenic belt, which contains abundant exposed mafic–ultramafic rocks (Qin et al., 2012). Eastern Tianshan located at the southern margin of the CAOB has better metallogenic conditions and it is an important base of nickel–copper resources in China based on accounting for 31.4% of the nickel resources in Xinjiang. The large-scale copper–nickel deposits formed in mafic–ultramafic rocks of the orogenic belt are one of the significant characteristics of Ni–Cu mineralization in eastern Tianshan. For example, Tulargen, Huangshan, Huangshandong, Xiangshan, Hulu, Erhongwa, and Tudun copper–nickel sulfide deposits are occurred along the Kanggur-Huangshan fault zone in eastern Tianshan and characterized by multistage intrusive bodies and distinct lithofacies (Mao et al., 2008; Qin et al., 2012; Wu et al., 2018), with a relative concentrative metallogenic age (290–275 Ma) (Sun et al., 2010, 2013b; Zhao et al., 2015; Chen et al., 2018; Feng et al., 2018). However, although the main ore-bearing mafic–ultramafic intrusions in eastern Tianshan have experienced sulfide segregation at depth, and still have different views on sulfur saturation mechanism about fractional crystallization and crustal contamination (Zhang et al., 2011; Sun et al., 2013b; Deng et al., 2014, 2015). Whether these mafic–ultramafic intrusions were related to the Tarim mantle plume (Mao et al., 2008; Pirajno et al., 2008; Qin et al., 2011; Tang et al., 2011; Zhang et al., 2017), subduction accretion (Mao et al., 2006b; Ao et al., 2010; Xue et al., 2016), or post-collisional extension setting is still being debated (Deng et al., 2011a, 2015; Gao et al., 2013; Sun et al., 2013b).

The Lubei Ni–Cu–Co deposit was newly discovered by the Geological Survey Academy of Xinjiang in 2014 during a geochemical anomaly inspection of the western segment in eastern Tianshan (Yang et al., 2017). The estimated reserve contains approximately 9.11 million tons of ore resources with an average grade of 0.82 wt% Ni, 0.52 wt% Cu, and 0.03 wt% Co. In particular, cobalt was reported as a critical metal for the first time. The Lubei intrusions were distributed in northern Kanggur fault and emplaced into the tuffaceous clastic rocks in the early Carboniferous Xiaorequanzi Formation (Yang et al., 2017; Li and Tian, 2018). The age of the zircon U–Pb from hornblende gabbro is 287.9 ± 1.6 Ma (Chen et al., 2018). However, there are few researches on the critical mechanisms of sulfur saturation and mineralization processes during migration of the magmas in their conduit system. The prospecting and exploration studies are still in progress. A great breakthrough in the northern mining area in 2020 made the systematic studies of magmatic evolution and mineralization mechanism more practical. Based on the fine identification of magmatic lithofacies, this contribution intends to restrict the metallogenic section, magma source, and sulfur saturation mechanisms in the magma conduit system using petrology and Sr–Nd–Hf isotopic evaluation of the Lubei intrusion. Combined with the regional geological data, we try to reconstructed the tectonic evolution, magmatic differentiation, and mineralization process in the magma conduit system of the Lubei Ni–Cu deposit, hope to provide the theoretical supporting for future Ni–Cu–Co deposit prospecting in eastern Tianshan.

GEOLOGICAL SETTING

The northern Xinjiang region located at the southern margin of the CAOB is adjacent to the Siberian Craton to the north and the Tarim Craton to the south (**Figure 1A**), which distributes different types of Ni–Cu deposits formed in orogenic belt. The Kalatongke Ni–Cu deposit related to post-collisional extension is located in southern Altay (Zhang et al., 2005), whereas the Jingbulake deposit related to the subduction of the southern Tianshan Ocean is distributed in western Tianshan (Zhang et al., 2012). The Poyi and Poshi deposits related to the Tarim mantle plume in the Permian are distributed in Beishan (Su et al., 2013a; **Figure 1B**). The eastern Tianshan is successively divided into the Dananhu-Tousuquan island arc, Jueluotage belt, and Central Tianshan block from north to south, bounded by the Kanggur and Aqikekuduk faults (**Figure 1C**).

The northern portion of the Dananhu-Tousuquan island arc is characterized by Paleozoic Kalatage arc volcanic rocks and pyroclastic rocks which intercalated with marine intermediate-felsic volcanic sedimentary rocks. Along with gradually weakened volcanic activities from Ordovician to Devonian, the magma compositions gradually transited from intermediate-basic to intermediate-acidic and accompanied by extensive granitic intrusive magmatism. In the early Carboniferous, the andesitic and dacitic tuffs of the Xiaorequanzi Formation and Qi'eshan Formation were distributed on the northern Kanggur fault. In the late Carboniferous, the gradually weakened volcanism was accompanied by shallow marine terrigenous clastic rocks. In the early Permian, bimodal volcanic rocks occurred in some areas, while the continental fluvial-lacustrine sediments were dominant in the late Permian (Long et al., 2019). In addition, mafic–ultramafic rocks were scattered and formed the Baixintan (Zhao et al., 2018), Yueyawan (Sun et al., 2019), and Lubei (Chen et al., 2018) Cu–Ni (–Co) deposits.

The Jueluotage tectonic belt in eastern Tianshan can be divided into the Kanggur-Huangshan ductile shear zone and the Aqishan-Yamansu island arc bounded by the Yamansu fault (**Figure 1C**). The Kanggur-Huangshan belt is influenced by the Kanggur-Huangshan ductile shear, which formed a set of disordered strata with strong deformation and metamorphism in the Carboniferous. The Aqishan-Yamansu belt is mainly composed of early Carboniferous intermediate-acidic island arc volcanic rocks, shallow marine carbonate rocks intercalated with clastic rocks, and late Carboniferous continental volcanic sedimentary rocks, with molasse formation at the top of Permian.

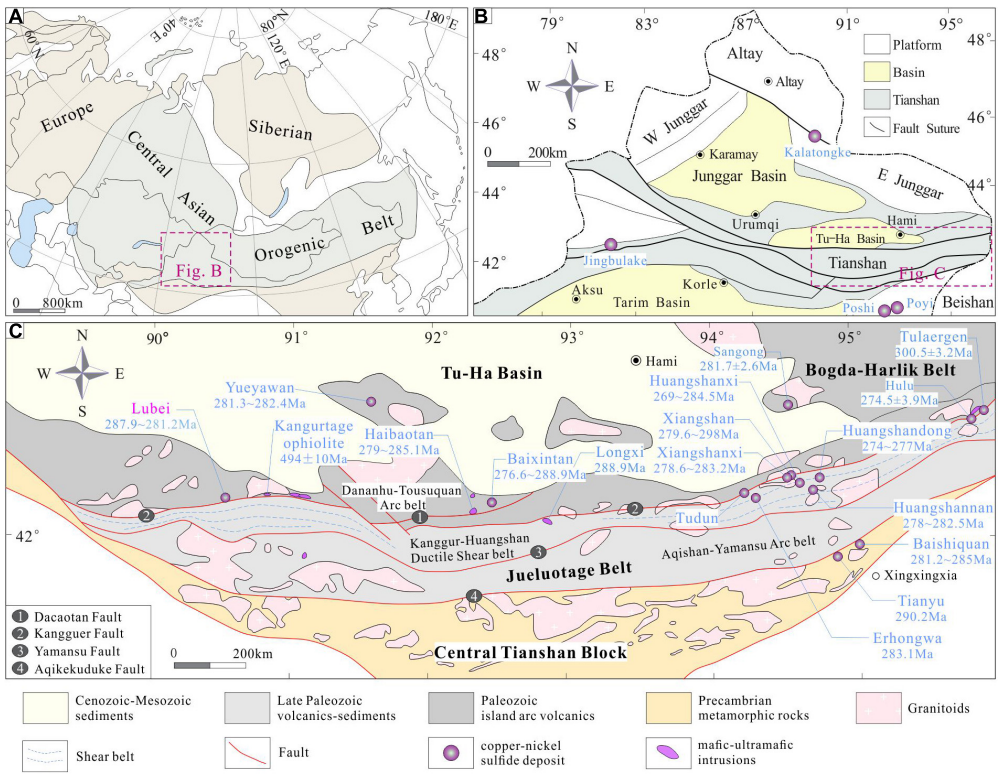

FIGURE 1 | (A) Simplified map of the CAOB; **(B)** Tectonic framework and representative Ni–Cu sulfide ore deposits in northern Xinjiang; **(C)** Simplified geological map of the eastern Tianshan showing the distribution of early Permian mafic–ultramafic intrusions. See **Supplementary Appendix 1** for details on geochronology.

The ages of granites, diorite porphyrite, and mafic dykes respectively are about 349–246 Ma (Zhou et al., 2010), 315–311 Ma (Long et al., 2020), 260–290 Ma (Lin et al., 2014) within the Jueluotage tectonic belt.

The Central Tianshan Block is composed of clastic rocks, carbonate rocks, volcanic rocks, and intrusive rocks. Metamorphic rocks were developed widely, mainly include the Paleoproterozoic Tianhu Group, Mesoproterozoic Xingxingxia Group, and Kawabulake Group (Wang et al., 2017). The intrusive magmatism is dominated by granitic rocks with emplacement ages from the late Archean to Mesozoic. The Baishiquan and Tianyu Ni–Cu deposits related to the Permian mafic–ultramafic rocks were formed in the eastern part of the belt (Wu et al., 2005; Tang et al., 2011).

The mafic–ultramafic intrusions in eastern Tianshan mainly distributed along with the Kanggur-Huangshan deep fault in the form of beads. Before 2010, researchers were mainly focused on the geological background and exploration of the mafic–ultramafic complexes in the Huangshan-Tulargen metallogenic belt in the eastern part of the Jueluotage tectonic belt (Han et al., 2004; Zhou et al., 2004; Hu et al., 2008; Sun et al., 2010). More than 30 mafic–ultramafic rocks in different spatial scales were identified successively in the eastern segment of the Jueluotage tectonic belt, which hosted the Huangshan, Xiangshan, Hulu, Tulargen, Tudun, and Huangshannan Ni–Cu deposits (San et al., 2010; Qin et al., 2011; Zhao et al., 2015; **Supplementary Appendix 1**). In recent years, new Ni–Cu (–Co) deposits have been found in the western segment of the Jueluotage tectonic belt, such as the medium-scale Lubei and Baixintan deposits (Wang et al., 2015a; Yang et al., 2017). Moreover, Yang et al. (2017) identified more than 20 outcrops of mafic–ultramafic rocks in the Lubei mining area including peridotite, pyroxene peridotite, olivine gabbro, gabbro, etc. Most of the mafic–ultramafic rocks contain pentlandite, indicating good nickel–copper (–cobalt) prospects.

ORE DEPOSIT GEOLOGY

Geology

The Lubei intrusion is situated in northern Kanggur fault and was emplaced into the tuffaceous clastic rocks of the Xiaorequanzi Formation in the early Carboniferous, which are situated in a semiring shape on the plane with an exposure area of 1.35 km^2. The Lubei intrusion was divided into two parts, north and south. The southern part contains mafic–ultramafic rocks that occur in high-grade orebodies, which are composed of peridotite, pyroxene peridotite, olivine pyroxenite, minor gabbro, diorite, and quartz diorite. The surface length is approximately 2,000 m, the exposed width is from 400 to 800 m with an average of 500 m, and the area is 0.89 km^2. The northern part was composed of mafic rocks, the host rock of the low-grade orebody, primarily lithology are gabbro, hornblende gabbro, and minor diorite

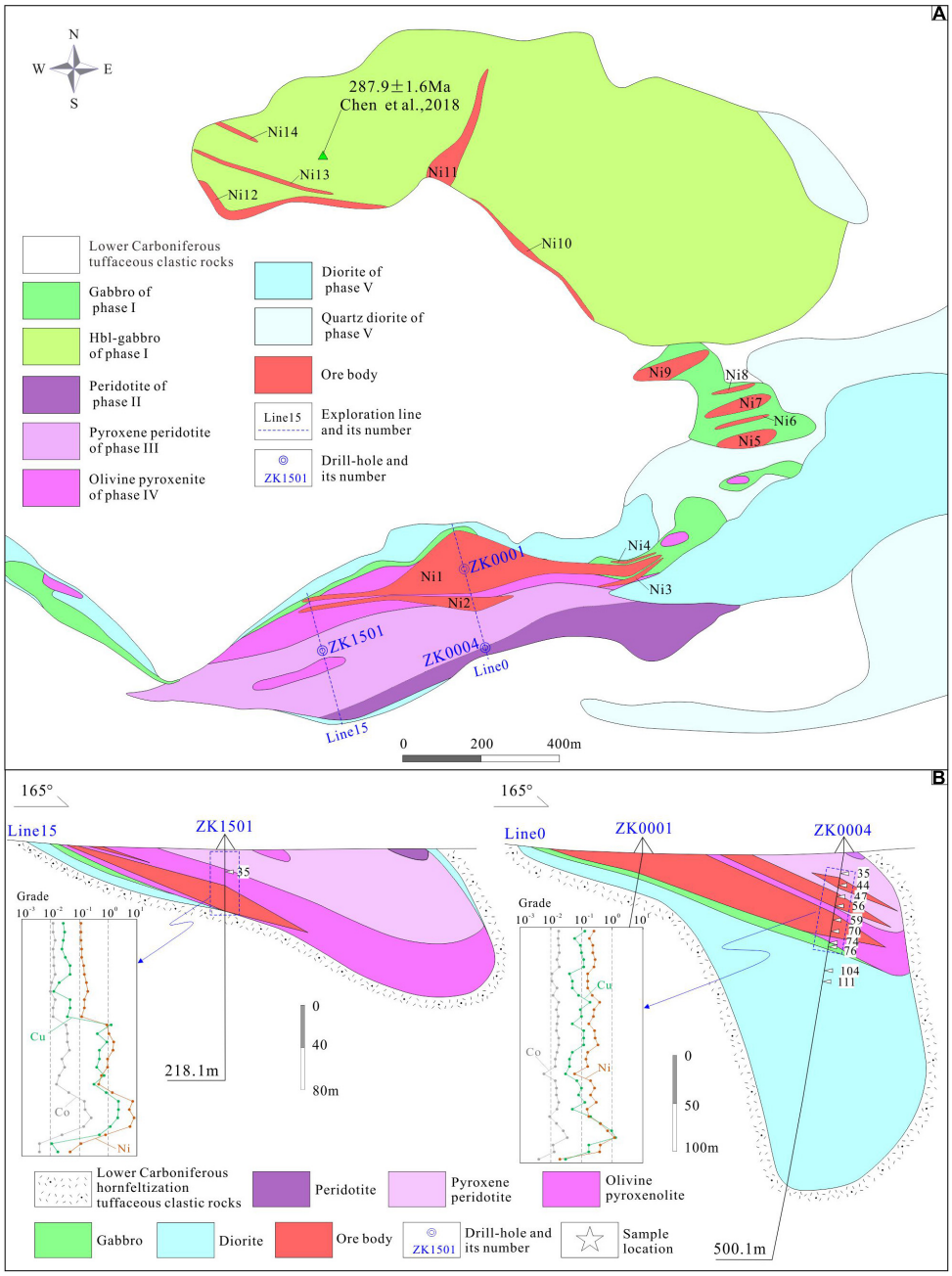

FIGURE 2 | Simplified geological map **(A)** and sample location **(B)** of the Lubei intrusion and Ni–Cu–Co orebodies.

(**Figure 2A**). The surrounding rocks are emplaced by the Lubei intrusion heated into hornfels.

Petrology

According to the spatial distribution, the mineral assemblage, the mineralization, and the alteration, the Lubei intrusion can be divided into five intrusive sequences: gabbro → peridotite → pyroxene peridotite → olivine pyroxenite (**Figure 3A**) → diorite (**Figures 3B,C**). The details of the characteristics for each lithology are described as follows:

The gabbro (phase I) is one of the ore-bearing rocks, includes gabbro and hornblende gabbro. Gabbro distributes at the edge of pyroxenite in the southern portion of the mining area, mainly represented by No. 4 to No. 9 orebodies with weak mineralization of nickel–copper–cobalt. The gabbro is composed of clinopyroxene (25%±), plagioclase (70%±), and olivine. Plagioclase with kaolinization has a particle size of 0.12–0.6 mm. Hornblende gabbro only distributes in northern part of the mining area with average of 287.9 ± 1.6 Ma (Chen et al., 2018) and mainly forms ore bodies No. 10 to No. 14.

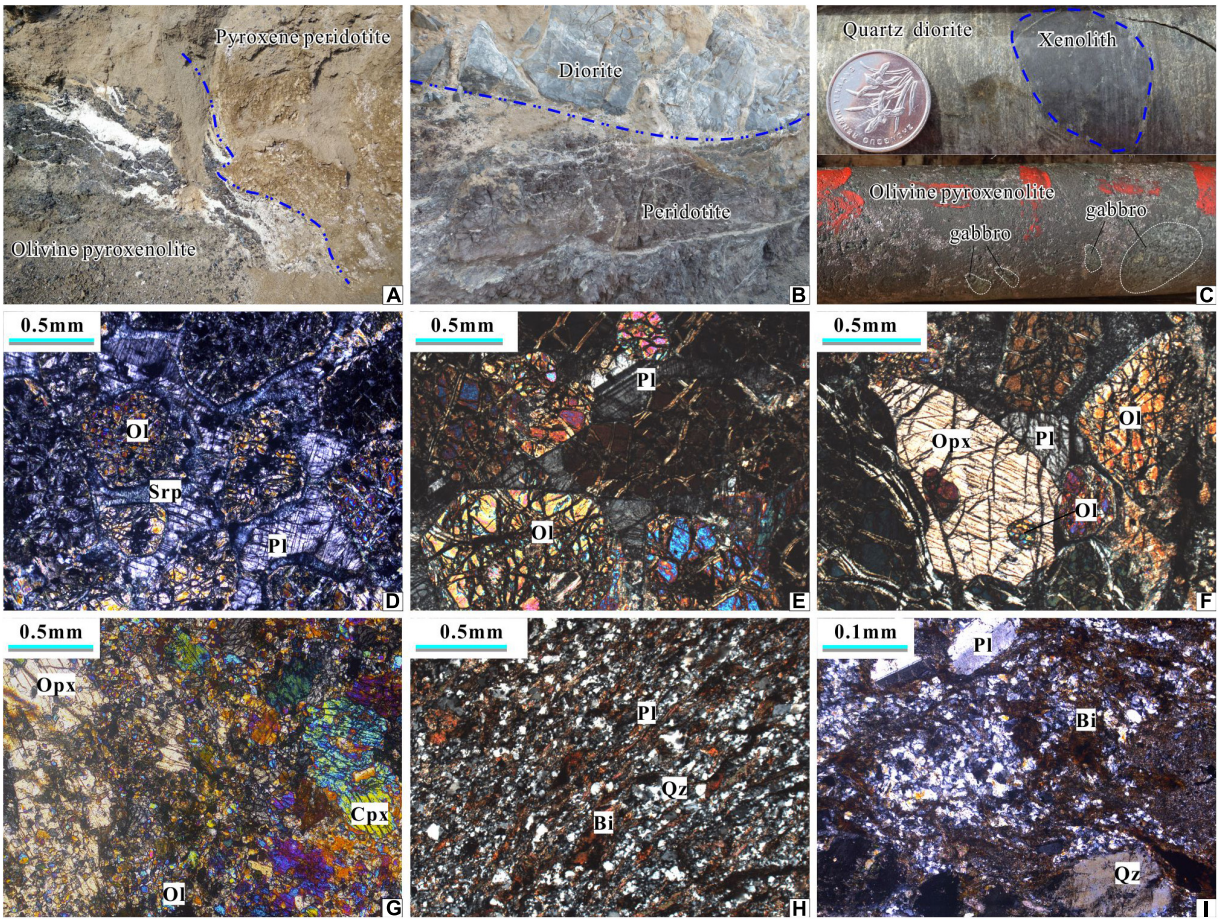

FIGURE 3 | Photos of outcrops and microphotographs of representative rocks from Lubei deposit. **(A)** contact relationship between olivine pyroxenite and pyroxene peridotite; **(B)** contact relationship between diorite and peridotite; **(C)** wall–rock xenoliths in quartz diorite and gabbro xenoliths in olivine pyroxenite; **(D)** serpentinized peridotite; **(E)** pyroxene peridotite; **(F)** pyroxene peridotite; **(G)** fragmented olivine pyroxenite; **(H)** slightly deformed quartz diorite; **(I)** deformed quartz diorite with porphyritic texture. Ol, olivine; Opx, orthopyroxene; Cpx, clinopyroxene; Pl, plagioclase; Srp, serpentine; Bi, Biotite; Qz, quartz.

The peridotite (phase II) only situated in southernmost part of the Lubei intrusion that intruded by the diorite (**Figure 3B**). The rock shows strong iddingsite, serpentinization (**Figure 3D**), and carbonate alteration without Ni–Cu–Co mineralization, and contains olivine (62%±), serpentine (25%±), calcite (10%±), and magnetite (3%±) (**Figure 3E**). The olivine characterized by network cracks is hypidiomorphic with a width of 0.3–1 mm and is filled with serpentine along the edge.

The pyroxene peridotite (phase III) only situated in south of the Lubei intrusion, which is obviously different from olivine pyroxenite and forms ore body No. 2. The rocks are serpentinized and glided and are mainly composed of olivine (62%±), augite (15%±), and serpentine (15%±) (**Figure 3F**). The Olivine exists in euhedral and subhedral grains, with a particle size of 0.5–1.5 mm. Augite in the form of subhedral columnar distributes between olivine, with a particle size of 0.5–1 mm. Serpentine distributes between olivine and pyroxene in fibrous form. Calcite distributes in the vein along the edges of fractures in olivine.

The olivine pyroxenite facies (phase IV) mainly situated in the southern mining area, intruded by diorite and exposed sporadically. It is the most important ore bearing rock which is formed by the largest No.1 ore body. The rocks are mainly composed of olivine (10%±), orthopyroxene (43%±), and clinopyroxene (25%±), occasionally accompanied with olivine, amphibolite, and chloritization (**Figure 3G**). The Olivine has a xenomorphic granular structure with a particle size of 0.28 ± 2.3 mm, and the orthopyroxene is columnar with a particle size of 0.24 ± 3.2 mm.

The diorite (phase V) mainly situated at the edge and along the underpart of the Lubei intrusion, represents the latest product with wallrock xenoliths (**Figure 3C**). The rocks are composed of plagioclase (75%±), amphibole (15%±), quartz (10%±), and deformed minor biotite (**Figure 3H**), magnetite, and porphyritic textures (**Figure 3I**). Plagioclase has a euhedral plate structure, slightly kaolinized with a particle size of 0.4–2 mm. Amphibole is actinolitice, distributes between plagioclase crystals. Biotite distributes between plagioclase crystals in a leaf shape. Magnetite distributes between hornblende and plagioclase in xenomorphic granular form.

Mineralization

There are 14 identified orebodies in the Lubei deposit, includes orebodies Nos. 1–4 in southern part which mainly hosted by olivine pyroxenite, orebodies Nos. 5–9 in the middle part that mainly occur in the gabbros, and orebodies Nos. 10–14 in the northern part that mainly occur in the hornblende gabbro (**Figure 2A**). The Ni–Cu–Co sulfide orebodies are bedded (**Figure 2B**) and dip south with a dip angle of 14°–28°. The No.1 orebody, as the largest ore body in the mining area, extends about 930 m at surface and 265 m in depth, and has average grades of 0.91%Ni, 0.54% Cu, and 0.031% Co. The main ore minerals include pentlandite, chalcopyrite, pyrrhotite, magnetite, and chromite. The ores in gabbro are mainly present as disseminated, and ores in olivine pyroxenite are mainly shown as massive (**Figures 4A–C**). Pentlandite and pyrrhotite coexist with chalcopyrite (**Figures 4D,F,G**). Chromite generally coexist with magnetite (**Figure 4E**) or surround pentlandite (**Figures 4J–M,O**). Pyrrhotite shows strong oxidation (**Figures 4H,I,M,N**).

ANALYTICAL METHODS

Conducting backscattering image observation and mineral chemical composition analysis of ore minerals, using a JEOL JXA-8230 electron probe microanalyzer (EPMA) at Xinjiang Experimental Institute of Mineral Resources, the analytical conditions for component analysis were 15 kV, 10 nA beam current, 1–10 μm beam size, 10 s peak-counting time, and 5 s upper and lower background counting time.

Laser Ablation–Inductively Coupled Plasma–Mass Spectrometry (LA–MC–ICP–MS) zircon U–Pb analyses as has been completed in Nanjing FocuMS Technology Co., Ltd., by applying a laser-ablation inductively coupled plasma mass spectrometer with Agilent 7700X. The spot size was 24 μm, with standard zircon samples 91500, GJ-1, and NIST SRM 610. Weighted mean age calculations and concordia diagrams were processed by using ISOPLOT software (Ludwig, 2003).

Hf isotope analyses were conducted by using a multi-collector Thermo Electron Neptune MC–ICP–MS system at the same company as LA–MC–ICP–MS zircon U–Pb analyses. Helium was used as the carrier gas of denudation material in the experiment. Ablation protocal employed a spot diameter of 50 μm at 8 Hz repetition rate for 40 s. The zircon GJ-1 was used as external standard with the $^{176}Hf/^{177}Hf$ average value of 0.282008 ± 28 (2σ). The analysis process and correction are shown in Hou et al. (2007).

The whole-rock geochemical analysis was conducted at ALS Laboratory in Guangzhou. The main elements were analyzed by X-ray fluorescence spectrometer (pw4400), and the accuracy of analysis was better than 1%. FeO was determined by volumetric titration. Rare earth and trace elements were determined by plasma mass spectrometry (PE300D). The analytical accuracy was better than 5–10%.

The whole-rock Sr–Nd isotopic analysis was performed at Nanjing FocuMS Technology Co., Ltd., applied by a Nu plasma HR multi-collector plasma mass spectrometer. For Sr–Nd isotope analyses, rock powders (∼100 mg) were dissolved in distilled HF-HNO_3 Savillex screwtop Teflon beakers at 150°C overnight. Strontium and REEs were separated on columns which are made of Sr and REE resins from the Eichrom Company using 0.1% HNO_3 as eluant. Separation of Nd from the REE fractions was carried out on HDEHP columns with a 0.18 N HCl eluant. Measured Sr and Nd isotopic ratios were respectively normalized by using a $^{86}Sr/^{88}Sr$ value of 0.1194 and a $^{146}Nd/^{144}Nd$ value of 0.7219. The analyses of standards NIST SRM 987 for Sr and JNdi-1 for Nd over the measurement period respectively provided:$^{87}Sr/^{86}Sr$ = 0.710291 ± 6 (2σ), and $^{143}Nd/^{144}Nd$ = 0.512084 ± 3 (2σ).

ANALYTICAL RESULTS

Chemical Compositions of Major Minerals

The trace elements of the major minerals are shown in **Supplementary Appendix 2**. According to above observations and EPMA data, the characteristics of the maucherites are different from the disseminated and vein mineralization types. The pyrrhotite is composed of 60.176–63.394 wt% iron, 0.016–0.085 wt% cobalt, <0.078 wt% nickel, 35.76–39.263 wt% sulfur, and trace amounts of tellurium, copper, and arsenic. The pentlandite is composed of 28.443–32.981 wt% iron, 0.527–2.459 wt% cobalt, 31.307–36.737 wt% nickel, 32.843–33.803 wt% sulfur, and trace amounts of copper and arsenic. The tellurium of pentlandite from zk004-35, 44 ranges from 1.476 to 1.837 wt%. Copper and nickel minerals coexist with each other, and cobalt minerals appear in pentlandite as isomorphism.

LA–MC–ICP–MS U–Pb Zircon Dating

Because of the outcrops of the Lubei intrusion are weathered severely, the fresh diorite (phase V) sample was collected from the bottom of the Lubei intrusion in drill hole ZK004 for zircon U–Pb dating. The data are listed in **Supplementary Appendix 3**. The zircon in the diorite has 50–120 μm long and 40–60 μm width, and it was shown as a magmatic origin with oscillatory zoning. The zircon U content of 23 points ranges from 232.8 × 10^{-6} to 630.1 × 10^{-6}, and the Th content between is 130.1 × 10^{-6} and 509.2 × 10^{-6}, with a Th/U ratio of 0.53–0.85, which indicates the magmatic origin of zircon. The zircon concordant age is 281.3 ± 0.7 Ma (2σ, MSWD = 4.2), and the weighted mean age of $^{206}Pb/^{238}U$ is 281.2 ± 1.5 Ma (2σ, MSWD = 2.4) (**Figure 5A**). Therefore, the mean $^{206}Pb/^{238}U$ age is interpreted to be the crystallization age of the diorite (Li et al., 2018), and it represents the latest magmatism (phase V) of the Lubei intrusion. This age is consistent with that of mafic-ultramafic rocks in Lubei intrusion (Chen et al., 2018; Deng et al., 2020) and the typical mafic–ultramafic rocks in Huangshan, Huangshandong, and Xiangshan in the eastern Tianshan (**Figure 5B**).

Whole-Rock Geochemistry

The major and trace elements were analyzed as shown in phase I to phase V: (1) two gabbro samples (phase I), (2) two pyroxene peridotite samples (phase III), (3) five olivine pyroxenite samples (phase IV), and (4) two diorite samples

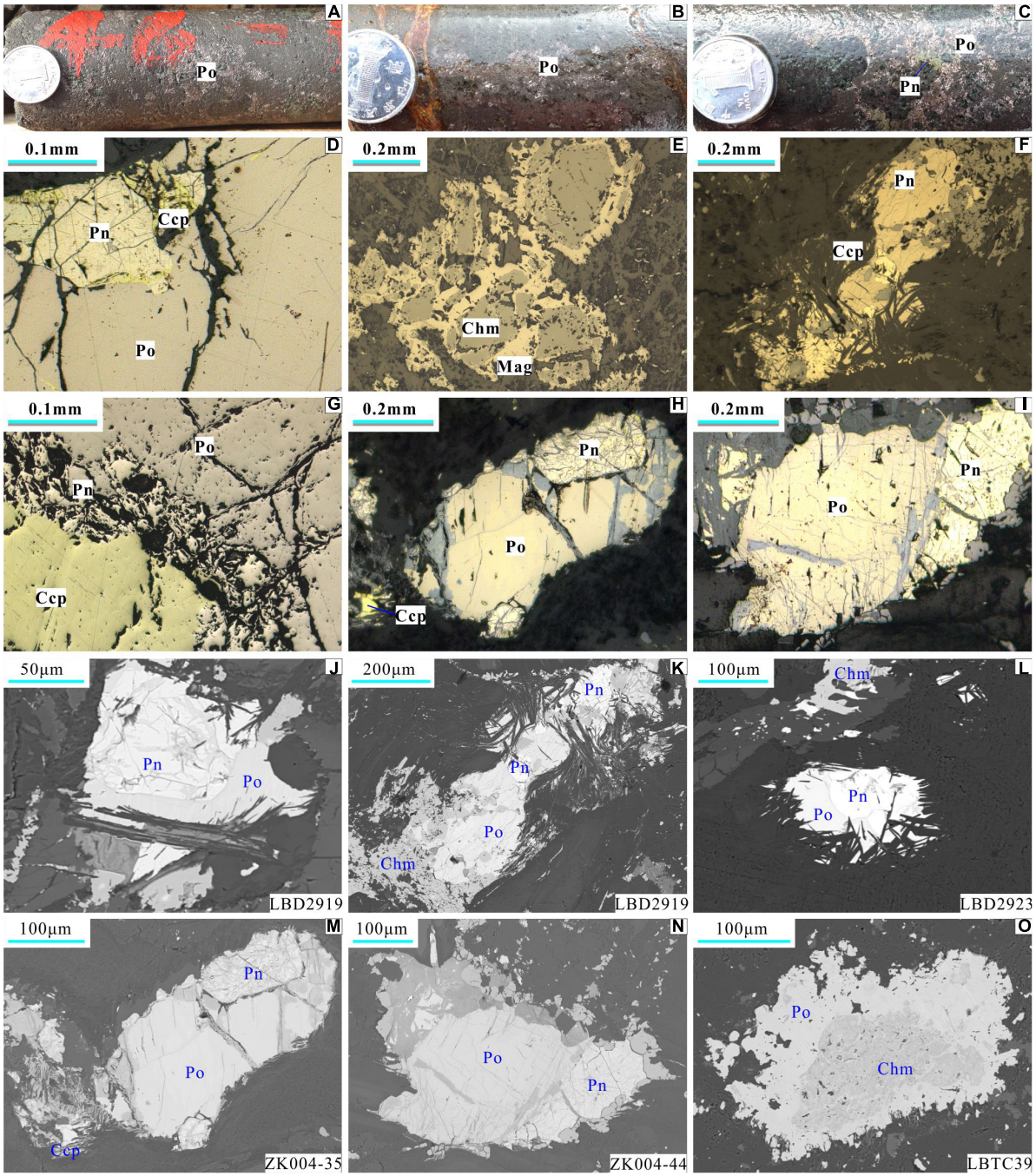

FIGURE 4 | Photos of outcrops and microphotographs of representative ores from Lubei deposit. **(A)** pentlandite in olivine pyroxenolite; **(B)** pentlandite in olivine pyroxenolite with limonitization vein; **(C)** Pn and Po in pyroxenolite; **(D)** Pn, Po, and Ccp co-occurrence; **(E)** Chm surrounded by Mag; **(F)** Pn coexisted with Ccp, and Pn in crack; **(G)** Pn, Po, and Ccp co-occurrence; **(H)** oxidized Po and Pn in crack; **(I)** oxidized Po; **(J)** Pn surrounded by Po; **(K)** Pn coexisted with Ccp, and Pn in crack; **(L)** Pn coexisted with Po; **(M)** oxidized Po and Pn in crack; **(N)** oxidized Po; **(O)** Chm surrounded by Po. Pn, Pentlandite; Po, Pyrrhotite; Chm, chromite; Ccp, chalcopyrite; Mag, magnetite.

(phase V) (**Supplementary Appendix 4**). The sample locations are shown in **Figure 2B**. Variable loss on ignition (LOI) values reflect variable degrees of alteration in the samples. Based on the plots and discussion below, the major element contents are normalized to 100% after the correction of LOI. Ultrabasic rocks in phase III and IV contain the lowest SiO_2 and Al_2O_3, and highest MgO and FeO^T contents. The Diorite of phase V exhibits the highest SiO_2 and Al_2O_3, and lowest MgO and FeO^T contents. The composition of gabbro in phase I is between ultrabasic rocks in phase III and IV and Diorite in phase V. All samples

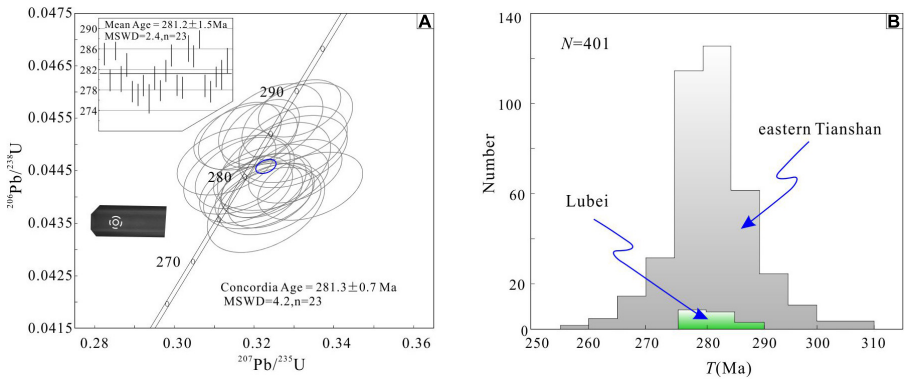

FIGURE 5 | Diagram of diagenetic age of Lubei diorite **(A)** and histogram of metallogenic age from Ni-Cu sulfide deposit in eastern Tianshan **(B)**. The data of eastern Tianshan from **Supplementary Appendix 1**.

of the Lubei intrusion are characterized by relatively low K_2O + Na_2O and TiO_2 contents. On the SiO_2 versus FeO^T/MgO diagram, the samples mainly fall into the field of tholeiite series (**Figure 6A**). On the (Mg+Fe)/Ti versus Si/Ti diagram, both pyroxene peridotite in phase III and pyroxenite in phase IV are on the control line of olivine and orthopyroxene, gabbro in phase I is on the control line of orthopyroxene and clinopyroxene, and diorite in phase V is on the control line of plagioclase (**Figure 6B**), which are consistent with the petrographic observation.

Total rare earth element (ΣREE) contents of the Lubei intrusion display an increasing trend from peridotite to gabbro, then to diorite (**Supplementary Appendix 4**), reflected an increase in the volume of inter cumulus liquids. The Lubei intrusion displays enriched light rare earth elements (LREEs) relative to heavy rare earth elements (HREEs) and lower LREE/HREE ratios. All the samples have a slightly negative Eu anomalies, with an average Eu/Eu* ratio of 0.89 (**Figure 6C**). Primitive mantle-normalized diagrams of incompatible elements also exhibit variable element concentrations (**Figure 6D**), the other notable features include the depletion of Nb and Ta relative to La and Th (**Figure 6D**). In particular, the distribution of the diorite is consistent with ultrabasic rocks, which indicates the diorite were evolved from homologous magma, and it is similar to typical Permian Ni–Cu sulfide deposits and mafic-ultramafic intrusions in the eastern Tianshan (**Figure 6D**).

Sr and Nd Isotopes

The results of the whole-rock Sr–Nd are summarized in **Supplementary Appendix 5**. The Rb concentration vary has a narrow range from 0.643×10^{-6} to 34.5×10^{-6}, whereas the Sr concentration ranges between 39.1×10^{-6} and 1171×10^{-6}. The initial $^{87}Sr/^{86}Sr$ ratios of the Lubei intrusion ranges from 0.704881 to 0.711383 with an average of 0.7073818. The value of $\varepsilon Nd_{(281Ma)}$ is -2.83 to +4.37, with an average value of +1.54. The Sr and Nd isotopic compositions indicate that the Lubei intrusion is characterized by low initial $^{87}Sr/^{86}Sr$ value and positive $\varepsilon Nd_{(281Ma)}$ value type magma source area (except for sample ZK004-59 with $\varepsilon Nd_{(281Ma)} = -2.83$), which is characterized by depleted mantle source area. The $\varepsilon Nd_{(281Ma)}$ value of −2.83 indicates the parental magma was contaminated by crustal materials.

Hf Isotopes

The results of zircon Hf isotope are summarized in **Supplementary Appendix 6**. The Lu–Hf isotopic compositions of zircon in diorite could be characterized as relatively high initial $^{176}Hf/^{177}Hf$ ratios (0.282916–0.282973, with an average of 0.282938) and slightly depleted εHf value (11.3–13.4, with an average of 12.1). Meanwhile, the zircon has relatively young one-stage model ages ($T_{DM(Hf)}$; 393–476 Ma), correspond to the T_{DM2} model ages which from 417 to 522 Ma. The narrow range of Hf isotopic compositions and slightly depleted εHf value indicates that the sources of these zircon grains were derived from depleted mantle, mixed with a small amount of crustal material.

DISCUSSION

Magma Source

The contact zone between the Lubei intrusion and country rock shows the contact metamorphism, and wall-rock xenoliths, and can be observed in the late emplaced diorite (**Figure 3B**), which indicates the Lubei intrusion experiences magmatic thermal emplacement instead of the ophiolite suite. At present, the mafic–ultramafic source of the eastern Tianshan Ni–Cu metallogenic belt is related to the Tarim large igneous province has become the focus (Xia et al., 2006; Pirajno et al., 2008). Large igneous provinces (LIPs) are characterized by large-scale mantle-derived magmatism occurring within a relatively short geological period (generally several Ma), mainly includes overflow basalts and radial basic dyke swarms (Coffin and Eldholm, 1994). The magma source was dominated by relatively dry and low volatile matter (Campbell and Griffiths, 1993). Most of the scholars believe that the mantle source of the Ni–Cu bearing mafic–ultramafic intrusions was modified by slab-derived melts and fluids due to oceanic crust subduction in eastern Tianshan before the Late Permian (Mao et al., 2008; Gao et al., 2013). However, there

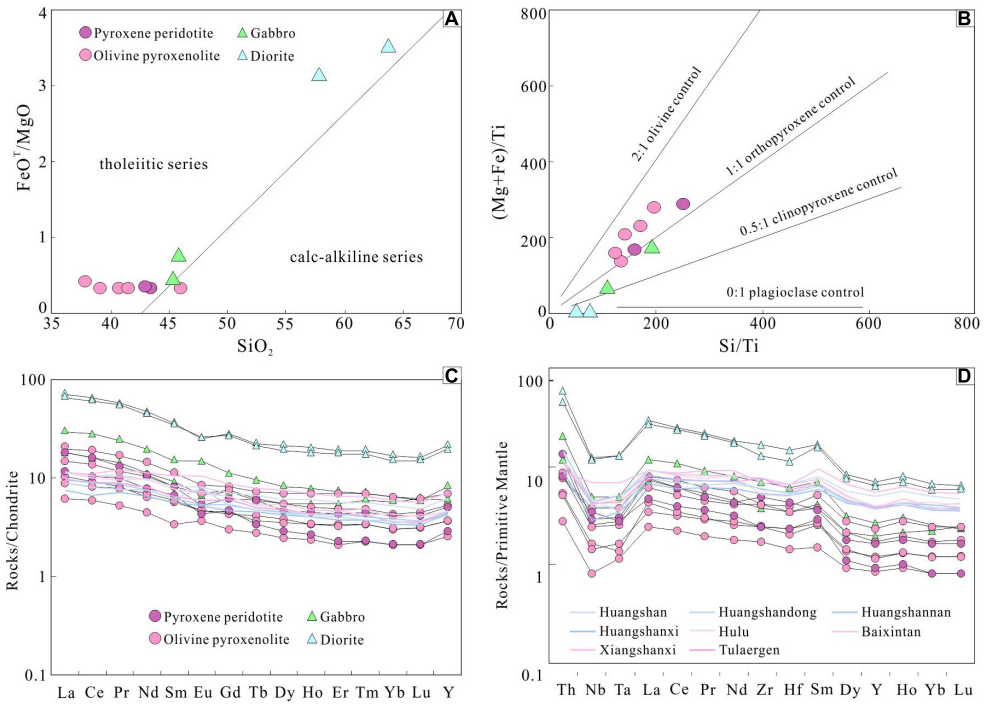

FIGURE 6 | Geochemical diagram of Lubei intrusion. Plot of SiO_2 versus FeO^T / MgO **(A)** and (Mg+Fe)/Ti versus Si/Ti **(B)**. chondrite– normalized REE patterns **(C)** and primitive mantle normalized trace element patterns **(D)** of the Lubei intrusion. The average data of line symbols are from **Supplementary Appendix 1**. Chondrite normalizing values are from Taylor and Mclennan (1985). Primitive mantle normalizing values are from Sun and McDonough (1989).

have had no reports on overflow basalts and radial basic dyke swarm assemblages related to LIPs in this area. On the contrary, amphibole, biotite, and other primary hydrous minerals are commonly found in the Lubei intrusion, which indicates that the primary magma related to subduction of Kanggur ocean basin in Late Carboniferous (Sun et al., 2020 and their references) is relatively wet.

The geochemical characteristics of the Lubei intrusion, which are relatively enriched in large ion lithophile elements (LILEs) (such as K, Rb, Ba, and Sr) and depleted in high field strength elements (HFSEs) (such as Th, Nb, Ta, and Ti), that indicate the magma suffered from fluid metasomatism during a subduction setting. In the $\varepsilon Nd_{(T)}$ versus $\varepsilon Hf_{(T)}$ diagram, the data points plot next to the ocean island basalt (OIB) and volcanic arc basalt (VAB; **Figure 7A**), which indicate the primary may be related to island arc magmatism. In the La/Nb versus La/Ba diagram, almost all samples plot in the subducted metasomatic lithospheric mantle region (**Figure 7C**). The $^{87}Sr/^{86}Sr$ versus $\varepsilon Nd_{(T)}$ diagram (**Figure 7B**) and Th/Zr versus Nb/Zr diagram (**Figure 7D**) indicate the fluids were involved in magmatic evolution. Due to the release of fluids from early altered slabs, many magmas in post–collisional extensional environments often inherits the magma source characteristics of fluid metasomatism in early subduction setting (Zhao et al., 2016), which is consistent with the low Nb and Ta concentrations of subduction-related magmas in the Lubei intrusion. All the results show that the magma source of the Lubei intrusion originated from the upwelling of the asthenosphere in a post-collisional extension setting, that led to the partial melting of metasomatic mantle which was modified by subduction fluid in the late Carboniferous (Deng et al., 2011b), and then formed to high magnesium tholeiite basaltic magma.

Ore Formation Mechanism

Ore formation mechanism generally has four ways which are: the changes in temperature and pressure, the fractional crystallization, the magma mixing, and the crustal contamination, that make magma reach sulfur saturation (Naldrett, 1999; Li and Ripley, 2005). First, the sulfur solubility decreases with decreasing temperature and increasing pressure (Li and Ripley, 2005). Although the initial magma is sulfur saturated, the sulfur will also be unsaturated during magma rise because of the increase in sulfur solubility, which is caused by the pressure drop is much greater than the temperature drop (Mavrogenes and O'Neill, 1999; Barnes and Lightfoot, 2005). Second, the sulfur content in the magma increases after the removal of Fe-oxide in fractional crystallization. Then, the magma became sulfur saturated and resulted in sulfide segregation (Haughton et al., 1974; Irvine, 1975). Third, magma mixing could change the saturation curve of sulfur and cause sulfur to enter the saturation zone to form immiscible sulfides (Irvine et al., 1983), such as the Bushveld and Jinchuan deposits. In fact, the petrology and geochemistry of the Lubei intrusion do not show the characteristics of magma mixing. Finally, crustal contamination was considered as a necessary factor for the formation of large Ni–Cu sulfide deposits (Naldrett, 2004, Naldrett, 2010).

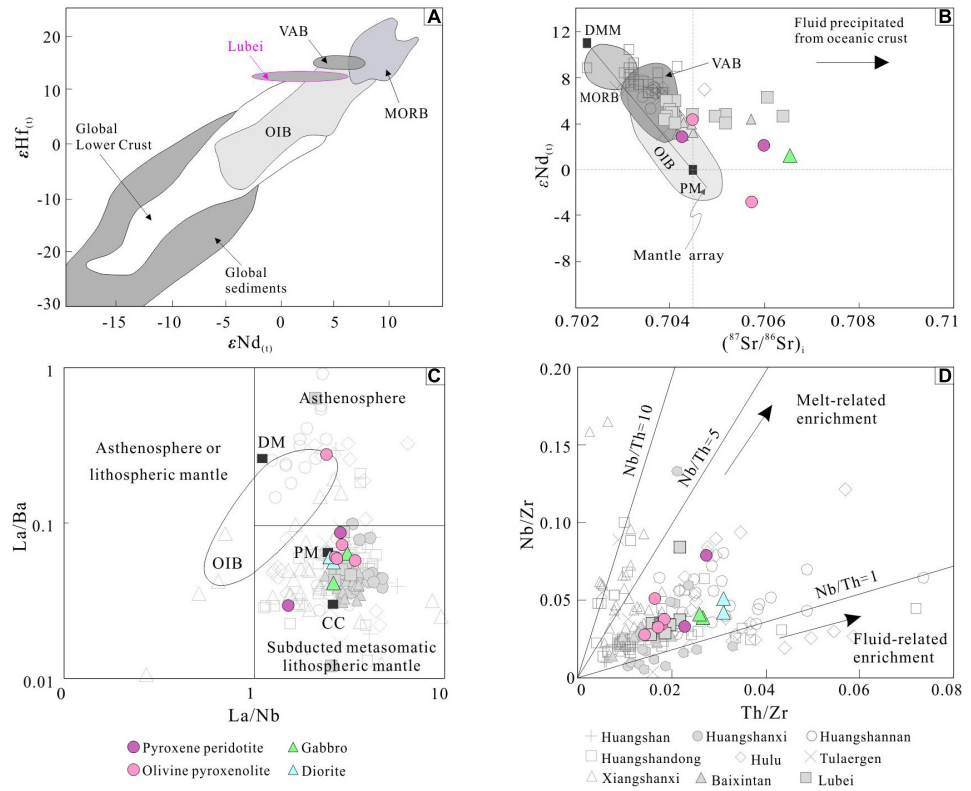

FIGURE 7 | Plot of $\varepsilon Nd_{(T)}$ versus $\varepsilon Hf_{(T)}$ **(A)**, $^{87}Sr/^{86}Sr$ versus $\varepsilon Nd_{(T)}$ **(B)**, La/Nb versus La/Ba **(C)**, and Th/Zr versus Nb/Zr **(D)**. The data of gray symbols are from **Supplementary Appendix 1**. Lower crust and sediments data from Bouvier et al. (2008) and Chauvel et al. (2014).

Fractional Crystallization

In addition, the gabbro at the edge was influenced by surrounding rocks in the early stage, the progressive decrease in olivine content from peridotite through orthopyroxene peridotite to olivine pyroxenite and the textures as described above indicate that the fractionation is dominated by the crystallization and accumulation of olivine, orthopyroxene and clinopyroxene, which is consistent with the mineral separation and crystallization control line (**Figure 6B**). The diorite samples plot on the trends are same as the other rocks of the intrusion. The diagrams of MgO versus major oxides and compatible elements (e.g., Cr and Co) illustrate the fractionation/accumulation of olivine, pyroxene, and plagioclase. For example, a negative correlation of MgO with SiO_2, CaO, Na_2O+K_2O, and TiO_2 indicates the fractionation/accumulation of clinopyroxene and plagioclase; a positive correlation of MgO with compatible elements (e.g., Cr, Co, Ni, and V) is consistent with the fractionation/accumulation of olivine and orthopyroxene (**Figure 8**).

Crustal Contamination

In fact, it is difficult to avoid the assimilation and contamination of magma from the mantle to the crust, and the key is the degree and source of crustal contamination. The source of crustal contamination includes the addition of silicon and sulfur materials. The former can reduce the solubility of sulfur in magma (Irvine, 1975; Lightfoot and Hawkesworth, 1997), and the latter can increase the sulfur content in magma (Lesher and Campbell, 1993). The sulfur saturation of some nickel–copper sulfide deposits is mainly caused by the addition of crustal SiO_2, and it has nothing to do with sulfur-rich surrounding rocks, such as Norilsk (Lightfoot and Hawkesworth, 1997; Ripley et al., 2003) and Kalatongke (Zhang et al., 2003) deposits. In addition, some sulfur-rich country rocks were incorporated into the magma to trigger sulfide saturation, such as Duluth and Voisey's Bay deposits (Lambert et al., 1998). The Hf isotopes of diorite deviate significantly from the depleted mantle evolution line (**Figure 9A**), which indicate that the diorite may have suffered from crustal contamination. The Rb/Sr ratio (0.04 to 0.47) of the Lubei intrusion varies greatly with $\varepsilon Sr_{(T)}$ value of 0.7–33.4. The Sr–Nd isotopic magma mixing simulation shows that the magma source suffered 4–10% lower crustal contamination with slight contamination of the upper crust (**Figure 9B**), which is similar to Tulargen (<5%, Jiao et al., 2012), Huangshangdong (5–8%, Xia et al., 2010), Erhongwa (<5%, Sun et al., 2013a), Hulu (5–10%, Xia, 2009) and Huangshannan (˜5%, Mao et al., 2016). The sulfur isotope $\delta^{34}S$ (−0.3 to +1.8‰, Chen et al., 2019) of the Lubei ores was characterized by mantle sulfur (−3 to +3‰; Ohmoto, 1986), which is consistent with the Huangshannan (−0.4 to +0.8‰, Mao et al., 2017) and Huangshanxi (−0.2 to +0.86‰, Zhang et al., 2011) deposits in eastern Tianshan. Therefore, we conclude that the main mechanism of sulfur saturation in Lubei

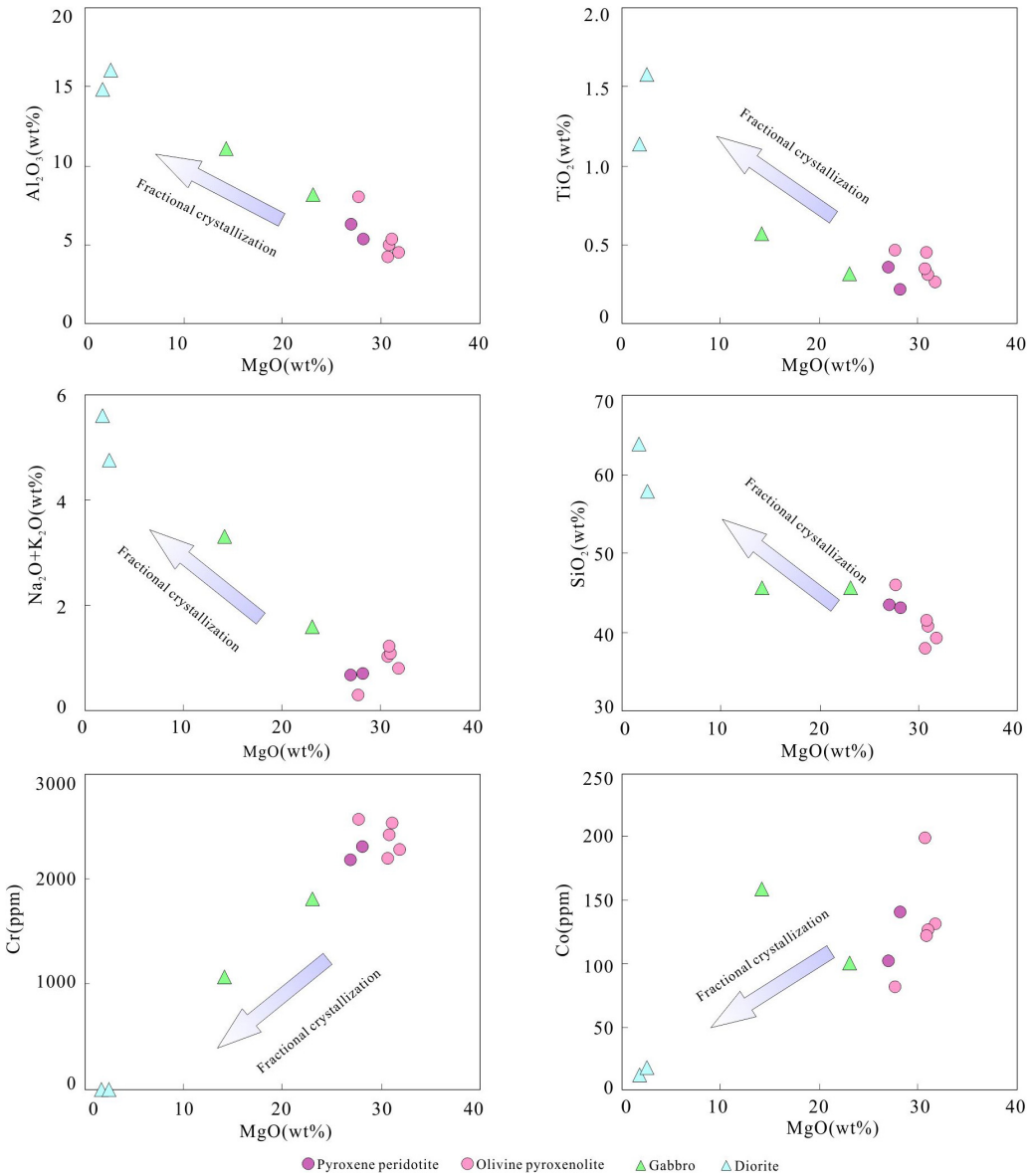

FIGURE 8 | Diagrams of MgO versus major oxides and compatible elements for the Lubei intrusion.

deposit is lower crustal contamination with slight contamination of the upper crust.

Metallogenic Process

The magma conduit plays an important role in the formation of Ni–Cu sulfide deposits (Maier et al., 2001; Su et al., 2014; Barnes et al., 2016). After the sulfur-unsaturated basaltic magma melt enters the crust, along with changes in temperature and pressure, and the addition of surrounding rock, sulfur saturation of magma is achieved through fractional crystallization and crustal contamination. Then, sulfide droplets are continuously deposited and accumulate owing to gravitational forces at the bend, widening, or bifurcation of the magma conduit due to the decrease in magma velocity (Keays, 1995; Naldrett, 1999; Lightfoot et al., 2012; Su et al., 2014). The Lubei Ni–Cu-Co sulfide deposit has undergone the following metallogenic processes (**Figure 10**).

The first stage is the formation of the parent magma. The high-Mg tholeiitic basaltic magma was formed by partial melting of the metasomatic lithospheric mantle (Chen et al., 2019), which was likely derived from a hydrous mantle previously modified by a fluid phase during the dehydration of the descending slab (Chen et al., 2018). The initial magma with a small amount of sulfide droplet migrates upwards through the conduit of the early structural fracture and rapidly crystallizes to form gabbro (phase I), influenced by the relatively low-temperature country rocks. The second stage is the fractional crystallization of the silicate and oxide minerals. As the magma moves upwards

within the conduit, the temperature gradually drops, and high-temperature minerals (such as olivine, orthopyroxene, etc.) begin to crystallize, which removes a large amount of Si, Mg, and Fe. Meanwhile, the addition of a small amount of wall rock materials will change the magma viscosity, sulfur solubility, and crystallization temperature. The sulfur solubility will decrease with decreasing FeO contents and increasing Si-rich materials (Irvine, 1975; Lightfoot and Hawkesworth, 1997), which can promote more metal elements into sulfide melts to gather gradually as sulfide droplets (Barnes et al., 2016). The third stage is crustal contamination and mineralization. The addition of abundant Si materials further reduced the sulfur solubility and forms abundant sulfides. Meanwhile, due to the addition of SiO_2, Al_2O_3, and volatiles, the flow velocity of magma slows to ensure adequate sulfide melt enrichment. The last stage is sulfide segregation and mineralization. Due to gravity flow and sulfide accumulation, the upper hanging ore body composed of disseminated ore generally forms in the middle of the magma, whereas the layered orebody composed of dense disseminated and dense massive ores forms in the lower part of the magma.

Geodynamic Setting

The crystallization age of the earliest emplacement of hornblende gabbro in the Lubei intrusion was 288 ± 1.8 Ma (Chen et al., 2018), and the latest emplacement diorite was 281.2 ± 1.5 Ma (Li et al., 2018), whose section (288–281 Ma) is consistent with the metallogenic ages of Huangshan, Huangshan, Xiangshan and other typical Ni–Cu–(Co) deposits in the eastern Tianshan area. At present, there are three different views of the geodynamic setting that formed the early Permian mafic–ultramafic

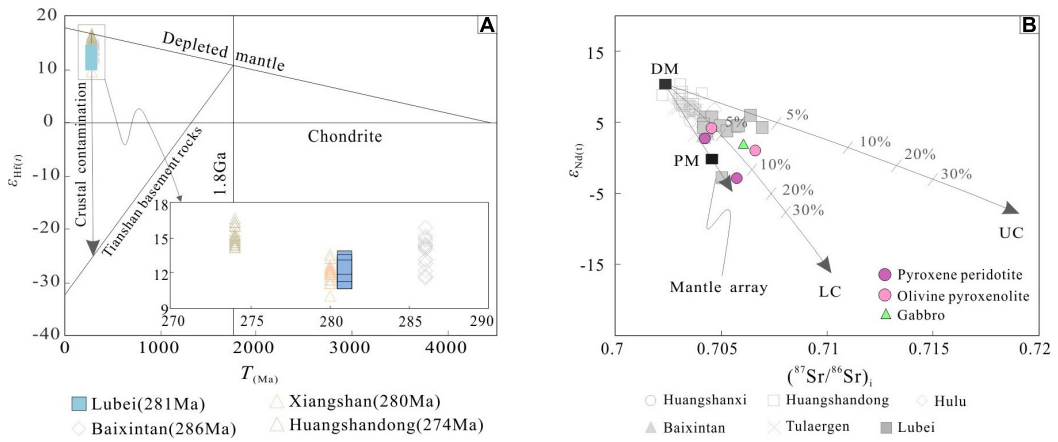

FIGURE 9 | Diagram of Hf **(A)** and Sr, Nd **(B)** isotopic crustal contamination tracing. LC and UC data from Rudnick and Gao (2011). The data of gray symbols are from **Supplementary Appendix 1**.

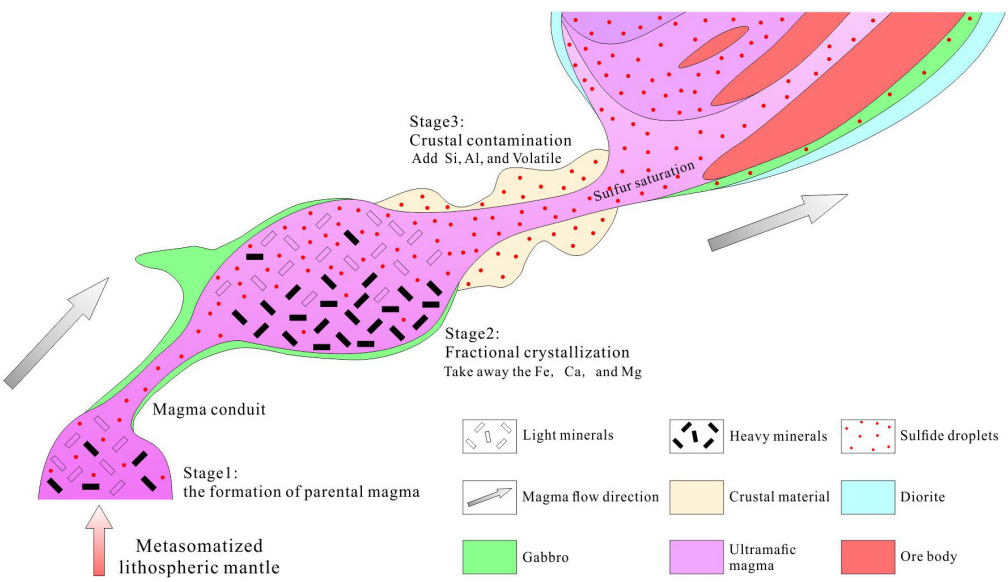

FIGURE 10 | Schematic diagram of pipeline facies mineralization model of Lubei Ni–Cu–Co sulfide deposit (modified from Barnes et al., 2016).

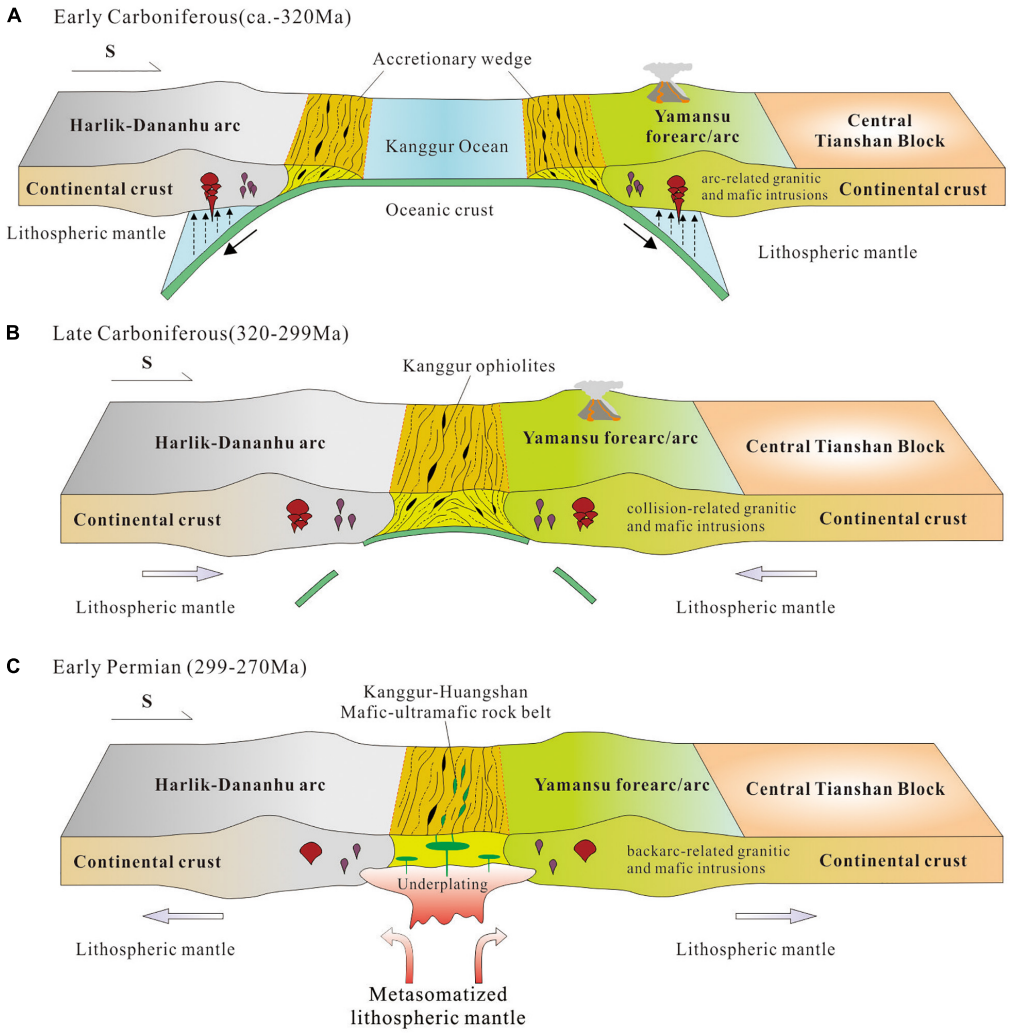

FIGURE 11 | The tectonic evolution in the late Paleozoic of eastern Tianshan. **(A)** the two-way subduction and accretion of the Kangur ocean basin occurred in the Early Carboniferous; **(B)** closure of Kanggur ocean basin in Late Carboniferous; **(C)** post-collisional extensional environment in Early Permian.

intrusions in the Huangshan-Jingerquan belt, including an active continental margin (Xiao et al., 2004; Mao et al., 2006b), a post-collisional lithosphere extension environment (Gu et al., 2006), and a mantle plume (Mao et al., 2006a; Pirajno et al., 2008; Su et al., 2013a). The geochemical characteristics of rocks suggest that the parent magma originated from a metasomatic mantle that was modified by subduction events, which is not consistent with the characteristics of rock assemblages and magmas of the Alaskan type (Irvine, 1974; Helmy and El Mahallawi, 2003). It is also inconsistent with the large-scale mantle-derived magmatism formed by the mantle plume within a short time (1–2 Ma), tholeiitic magma series, dry mantle source, and very low volatile content (Campbell and Griffiths, 1993). Therefore, we believe that the Lubei Ni– Cu–Co deposit formed in an extensional postcollisional environment with the geochemical characteristics of an early-stage subducted metasomatic mantle, which has nothing to do with mantle plume activity (Deng et al., 2011a). The regional tectonic–magmatic evolution and mineralization have had experienced the following processes.

The Kanggur ocean basin had already opened in the late Cambrian (494 ± 10 Ma, Li et al., 2008) and then entered the stage of ocean basin evolution. With the earliest subduction northward in the Late Ordovician (Du et al., 2018; Sun et al., 2018), the Dananhu–Tousuquan island arc belt was formed and accompanied by porphyry copper deposits (Sun et al., 2018), epithermal copper deposits (431.8 ± 2.7Ma, Deng et al., 2016) and VMS-type zinc–copper deposits (434.2 ± 3.9Ma, Deng et al., 2016) in the Kalatage area. The Devonian subduction continued to the north and formed basaltic–andesite volcanic rocks (Du et al., 2019). In the early Carboniferous, the Aqishan–Yamansu forearc basin or island arc belt was formed by subduction southward (Han et al., 2019; Zhao et al., 2019; Liu et al., 2020; **Figure 11A**) with iron and lead–zinc deposits related

to volcanism (Hou et al., 2014). At the same time, porphyry copper deposits were formed by subduction to the north (Wang et al., 2016; Xiao et al., 2017). In the late Carboniferous, the Kanggur ocean basin was closed (**Figure 11B**), and the tectonic compression environment led to the formation of volcanic iron deposits (Zhao et al., 2017; Zhang et al., 2018), as well as ductile shear zone gold deposits (Wang et al., 2015b; Muhtar et al., 2020a). The geodynamic setting in the early Permian represented post-collisional extension setting (Muhtar et al., 2020b; **Figure 11C**). The metasomatic lithospheric mantle produced in the early subduction stage was partially melted, and the mantle-derived magma upwelling formed beaded mafic–ultramafic rocks along the Kanggur–Huangshan regional fault, accompanied by Huangshandong, Huangshannan, Hulu, Tulargen, Baixintan, and Lubei sulfide deposits (San et al., 2010; Sun et al., 2010; Chen et al., 2013, 2018; Zhao et al., 2015; Feng et al., 2018).

CONCLUSION

1. The Lubei mafic–ultramafic intrusion was composed of five lithofacies, including gabbro (phase I), peridotite (phase II), pyroxenite (phase III), olivine pyroxenite (phase IV), and diorite (phase V). In addition to pyroxene peridotite (phase III) and gabbro (phase I), the most important ore-bearing lithology is olivine pyroxenite (phase IV).
2. The Lubei intrusion was formed at the same time as the bearing Ni–Cu–Co sulfide mafic–ultramafic rocks in eastern Tianshan, and its metallogenic age was between 288 ± 1.8Ma of hornblende gabbro (phase I) and 281.3 ± 0.7Ma of diorite (phase V).
3. In addition to magmatic fractional crystallization, the most important mechanism of sulfur saturation in Lubei Ni–Cu–Co deposit is crustal contamination. The Sr–Nd isotope shows that the contamination degree of lower crustal materials is 4–10% with slight contamination of the upper crust.
4. The Lubei Ni–Cu–Co deposit was formed in post-collisional extensional setting of the CAOB during the early Permian. The primary magma derived from partial melting of metasomatized lithospheric mantle was formed Ni–Cu–Co sulfide deposit has gone through three stages, including fractional crystallization, crustal contamination, and sulfide segregation.

DATA AVAILABILITY STATEMENT

The original contributions presented in the study are included in the article/**Supplementary Material**, further inquiries can be directed to the corresponding author/s.

AUTHOR CONTRIBUTIONS

PL: investigation, analysis, writing, and original draft preparation. TL: academic support and revising original version. YF: original manuscript English editing. TZ, JT, and DL: investigation and original figures editing. GC: investigation and financial support. JL: mineralogy analysis and interpretation. CW: geochemistry analysis and interpretation. All authors have contributed to the article and approved the submitted version.

FUNDING

This work was funded by the Project of China Geological Survey (Grant No. DD20190379), the National key R&D project of China (Grant No. 2018YFC0604001-04), and the second Tibetan Plateau Scientific Expedition and Research (Grant No. 2019QZKK0806).

ACKNOWLEDGMENTS

We thank Qiong Han, Liuyuan Jin, and Xiaojun Zhang from Geological Survey Academy of Xinjiang for assistance in fieldwork and thank the reviewers for providing critical comments and suggestions.

SUPPLEMENTARY MATERIAL

The Supplementary Material for this article can be found online at: https://www.frontiersin.org/articles/10.3389/feart.2021.648122/full#supplementary-material

REFERENCES

Ao, S. J., Xiao, W. J., Han, C. M., Mao, Q. G., and Zhang, J. E. (2010). Geochronology and geochemistry of early Permian mafic–ultramafic complexes in the Beishan area, Xinjiang, NW China: implications for late Paleozoic tectonic evolution of the southern Altaid. *Gondwana Res.* 18, 466–478. doi: 10.1016/j.gr.2010.01.004

Barnes, S. J., Cruden, A. R., Arndt, N., and Saumur, B. M. (2016). The mineral system approach applied to magmatic Ni–Cu–PGE sulphide deposits. *Ore Geol. Rev.* 76, 296–316. doi: 10.1016/j.oregeorev.2015.06.012

Barnes, S. J., and Lightfoot, P. C. (2005). "Formation of magmatic nickel sulfide ore deposits and processes affecting their copper and platinum group element contents," in *Economic Geology, 100th Anniversary Volume*, eds J. W. Hedenquist, J. F. H. Thompson, R. J. Goldfarb, and J. P. Richards (Littleton, CO: Society of Economic Geologists, Inc), 179–213.

Begg, G. C., Hronsky, J. A. M., Arndt, N. T., Griffin, W. L., O'Reilly, S. Y., and Hayward, N. (2010). Lithospheric, cratonic and geodynamic setting of Ni–Cu–PGE sulfide deposits. *Econ. Geol.* 105, 1057–1070. doi: 10.2113/econgeo.105.6.1057

Bouvier, A., Vervoort, J. D., and Patchett, P. J. (2008). The Lu–Hf and Sm–Nd isotopic composition of CHUR: constraints from unequilibrated chondrites and implications for the bulk composition of terrestrial planets. *Earth Planet. Sci. Lett.* 273, 48–57. doi: 10.1016/j.epsl.2008.06.010

Campbell, I. H., and Griffiths, R. W. (1993). The evolution of the mantle's chemical structure. *Lithos* 30, 389–399. doi: 10.1016/0024-4937(93)90047-g

Chauvel, C., Garçon, M., Bureau, S., Besnault, A., Jahn, B., and Ding, Z. L. (2014). Constraints from loess on the Hf–Nd isotopic composition of the upper

continental crust. *Earth Planet. Sci. Lett.* 388, 48–58. doi: 10.1016/j.epsl.2013.11.045

Chen, B. Y., Yu, J. J., and Liu, S. J. (2018). Source characteristics and tectonic setting of mafic–ultramafic intrusions in North Xinjiang, NW China: insights from the petrology and geochemistry of the Lubei mafic–ultramafic intrusion. *Lithos* 308–309, 329–345. doi: 10.1016/j.lithos.2018.03.016

Chen, B. Y., Yu, J. J., Liu, S. J., and Tian, J. T. (2019). Formation of the Lubei magmatic Ni–Cu deposit in a post–subduction setting in East Tianshan, North West China. *Ore Geol. Rev.* 104, 356–372. doi: 10.1016/j.oregeorev.2018.11.017

Chen, J. P., Liao, Q. N., Zhang, X. H., Luo, T., Guo, D. B., and Hu, Z. C. (2013). Contrast of huangshandong and Xiangshan mafic–ultramafic complex, East Tianshan. *Earth Sci. J. China Univ. Geosci.* 38, 1183–1196. doi: 10.3799/dqkx.2013.117

Coffin, M. F., and Eldholm, O. (1994). Large igneous provinces: crustal structure, dimensions, and external consequences. *Rev. Geophys.* 32, 1–36. doi: 10.1029/93RG02508

Deng, X. H., Wang, J. B., Pirajno, F., Wang, Y. W., Li, Y. C., Li, C., et al. (2016). Re–Os dating of chalcopyrite from selected mineral deposits in the Kalatag district in the eastern Tianshan Orogen, China. *Ore Geol. Rev.* 77, 72–81. doi: 10.1016/j.oregeorev.2016.01.014

Deng, Y. F., Song, X. Y., Chen, L. M., Cheng, S. L., Zhang, X. L., and Li, J. (2011a). Features of the mantle source of the Huangshanxi Ni–Cu sulfide–bearing mafic–ultramafic intrusion, eastern Tianshan. *Acta Petrol. Sin.* 27, 3640–3652. doi: 10.1080/00288306.2011.590212

Deng, Y. F., Song, X. Y., Chen, L. M., Zhou, T. F., Pirajno, F., Yuan, F., et al. (2014). Geochemistry of the Huangshandong Ni–Cu deposit in northwestern China: implications for the formation of magmatic sulfide mineralization in orogenic belts. *Ore Geol. Rev.* 56, 181–198. doi: 10.1016/j.oregeorev.2013.08.012

Deng, Y. F., Song, X. Y., Hollings, P., Zhou, T. F., Yuan, F., Chen, L. M., et al. (2015). Role of asthenosphere and lithosphere in the genesis of the Early Permian Huangshan mafic–ultramafic intrusion in the Northern Tianshan, NW China. *Lithos* 227, 241–254. doi: 10.1016/j.lithos.2015.04.014

Deng, Y. F., Song, X. Y., Jie, W., Cheng, S. L., and Li, J. (2011b). Petrogenesis of the Huangshandong Ni-Cu sulfide-bearing mafic-ultramafic intrusion, northern Tianshan, Xinjiang: evidence from major and trace elements and Sr-Nd isotope. *Acta Geol. Sin.* 85, 1435–1451.

Deng, Y. F., Song, X. Y., Jie, W., Yang, F., Zhao, Z. M., Wei, S., et al. (2021). Determination of sedimentary ages of strata in the Huangshan-Jingerquan mineralization belt and its geological significance. *Acta Geol. Sin.* 95, 362–376.

Du, L., Long, X. P., Yuan, C., Zhang, Y. Y., Huang, Z. Y., Sun, M., et al. (2018). Early Paleozoic dioritic and granitic plutons in the Eastern Tianshan Orogenic Belt, NW China: constraints on the initiation of a magmatic arc in the southern Central Asian Orogenic Belt. *J. Asian Earth Sci.* 153, 139–153. doi: 10.1016/j.jseaes.2017.03.026

Du, L., Zhang, Y. Y., Huang, Z. Y., Li, X. P., Yuan, C., Wu, B., et al. (2019). Devonian to carboniferous tectonic evolution of the Kangguer Ocean in the Eastern Tianshan, NW China: insights from three episodes of granitoids. *Lithos* 35, 1–11. doi: 10.1016/j.lithos.2019.105243

Feng, Y. Q., Qian, Z. Z., Duan, J., Xu, G., Ren, M., and Jiang, C. (2018). Geochronological and geochemical study of the Baixintan magmatic Ni–Cu sulphide deposit: new implications for the exploration potential in the western part of the East Tianshan nickel belt (NW China). *Ore Geol. Rev.* 95, 366–381. doi: 10.1016/j.oregeorev.2018.02.023

Gao, J. F., Zhou, M. F., Lightfoot, P. C., Wang, C. Y., and Qi, L. (2012). Origin of PGE–poor and Cu–rich magmatic sulfides from the Kalatongke deposit, Xinjiang, Northwest China. *Econ. Geol.* 107, 481–506. doi: 10.2113/econgeo.107.3.481

Gao, J. F., Zhou, M. F., Lightfoot, P. C., Wang, C. Y., Qi, L., and Sun, M. (2013). Sulfide saturation and magma emplacement in the formation of the Permian Huangshandong Ni–Cu sulfide deposit, Xinjiang, NW China. *Econ. Geol.* 108, 1833–1848. doi: 10.2113/econgeo.108.8.1833

Gu, L. X., Zhang, Z. Z., Wang, Y. X., Tang, J. H., Wang, C. S., Xi, A. H., et al. (2006). Some problems on granites and vertical growth of the continental crust in the eastern Tianshan Mountains, NW China. *Acta Petrol. Sin.* 22, 1103–1120.

Han, B. F., Ji, J. Q., Song, B., Chen, L. H., and Li, Z. H. (2004). SHRIMP zircon U–Pb ages of the Kalatongke and Huangshan East mafic complexes and their geological significance. *Sci. Bull.* 22, 2324–2328. doi: 10.1360/04wd0163

Han, J. S., Chen, H. Y., Jiang, H. J., Zhao, L. D., Zhang, W. F., and Lai, C. (2019). Genesis of the Paleozoic Aqishan–Yamansu arc–basin system and Fe (–Cu) mineralization in the Eastern Tianshan, NW China. *Ore Geol. Rev.* 105, 55–70. doi: 10.1016/j.oregeorev.2018.12.012

Haughton, D. R., Roeder, P. L., and Skinner, B. J. (1974). Solubility of sulfur in mafic magmas. *Econ. Geol* 69, 451–467. doi: 10.2113/gsecongeo.69.4.451

Helmy, H. M., and El Mahallawi, M. M. (2003). Gabbro Akarem mafic–ultramafic complex, Eastern Desert, Egypt: a late Precambrian analogue of Alaskan–type complexes. *Mineral. Petrol.* 77, 85–108. doi: 10.1007/s00710-001-0185-9

Hou, K. J., Li, Y. H., Zou, T. R., Qu, X. M., Shi, Y. R., and Xie, G. Q. (2007). Laser ablation-MC-ICP-MS technique for Hf isotope microanalysis of zircon and its geological applications. *Acta Petrol. Sin.* 23, 2595–2604. doi: 10.3969/j.issn.0371-5736.2013.02.017

Hou, T., Zhang, Z. C., Santosh, M., Encarnacion, J., Zhu, J., and Luo, W. J. (2014). Geochronology and geochemistry of submarine volcanic rocks in the Yamansu iron deposit, Eastern Tianshan Mountains, NW China: constraints on the metallogenesis. *Ore Geol. Rev.* 56, 487–502. doi: 10.1016/j.oregeorev.2013.03.008

Hu, K. B., Yao, S. Z., Qu, W. J., Du, A. D., and Ao, S. J. (2008). Re–Os isotopic analysis of the Hulu Cu–Ni sulfde deposit magmatic ore systme, Esat Tianshan, Xinjiang, NW China. *Acta Petrol. Sin.* 24, 2359–2370.

Irvine, T. N. (1974). Petrology of the Duke Island ultramafic complex southern Alaska. *Geol. Soc. Am. Memoir* 138:240. doi: 10.1130/mem138-p1

Irvine, T. N. (1975). Crystallization sequences in the Muskox intrusion and other layered intrusions; II, Origin of chromitite layers and similar deposits of other magmatic ores. *Geochim.; Cosmochim. Acta* 39, 991–1020. doi: 10.1016/B978-0-08-019954-2.50022-6

Irvine, T. N., Keith, D. W., and Todd, S. G. (1983). The J–M platinum–palladium reef of the Stillwater Complex, Montana: II, Origin by double diffusive convective magma mixing and implications for the Bushveld complex. *Econ. Geol.* 78, 1287–1334. doi: 10.2113/gsecongeo.78.7.1287

Jiao, J. G., Tang, Z. L., Qian, Z. Z., Sun, T., Duan, J., and Jiang, C. (2012). Genesis and metallogenic process of Tulargen large scale Cu–Ni sulfide deposit in eastern Tianshan area, Xinjiang. *Acta Petrol. Sin.* 28, 3772–3786.

Keays, R. R. (1995). The role of komatiitic and picritic magmatism and S–saturation in the formation of ore deposits. *Lithos* 34, 1–18. doi: 10.1016/0024-4937(95)90003-9

Lambert, D. D., Foster, J. G., Frick, L. R., Ripley, E. M., and Zientek, M. L. (1998). Geodynamics of magmatic Cu–Ni–PGE sulfide deposits: new insights from the Re– Os isotopic system. *Econ. Geol.* 93, 121–137. doi: 10.2113/gsecongeo.93.2.121

Lesher, C. M., and Campbell, I. H. (1993). Geochemical and fluid dynamic controls on the composition of Komatiite-hosted nickel sulfide ores in Western Australia. *Econ. Geol.* 88, 804–816.

Li, C., and Ripley, E. M. (2005). Empirical equations to predict the sulfur content of mafic magmas at sulfide saturation and applications to magmatic sulfide deposits. *Miner. Deposl.* 40, 218–230. doi: 10.1007/s00126-005-0478-8

Li, D. H., and Tian, J. T. (2018). Geological characteristics and Lithogeochemical features of Lubei Cu–Ni deposit, eastern Tianshan. *Xinjiang Geol.* 36, 423–428.

Li, P., Zhao, T. Y., Zhu, Z. X., Tian, J. T., and Li, D. H. (2018). First report of Zircon U–Pb ages from Lubei Cu–Ni Sulfide deposit in East Tianshan of central Asian Orogenic Belt (NW China). *Acta Geol. Sin. (Eng. Edition)* 92, 855–856. doi: 10.1111/1755-6724.13559

Li, W. Q., Ma, H. D., Wang, R., Wang, H., and Xia, B. (2008). SHRIMP dating and Nd– Sr isotopic tracing of Kangguertage ophiolite in eastern Tianshan, Xinjiang. *Acta Petrol. Sin.* 24, 773–780. doi: 10.1016/j.sedgeo.2008.03.004

Lightfoot, P. C., and Hawkesworth, C. J. (1997). "Flood basalts and magmatic Ni, Cu and PGE sulphide mineralization: comparative geochemistry of the Noril' sk (Siberian Trap) and West Greenland Sequences," in *Large Igneous Province*, eds J. J. Mahoney and M. F. Coffin (Washington DC: Amercian Geophysical Union), 357–380. doi: 10.1029/GM100p0357

Lightfoot, P. C., Keays, R. R., Evans–Lamswood, D., and Wheeler, R. (2012). S saturation history of Nain Plutonic Suite mafic intrusions: origin of the Voisey 's Bay Ni –Cu –Co sulfide deposit, Labrador, Canada. *Miner. Depos.* 47, 23–50. doi: 10.1007/s00126-011-0347-6

Lin, Y., Tang, Q. Y., Zhang, M. J., Jiao, J. G., Chen, S. T., and Hu, X. (2014). Magmstism and dynamic settings of Permian mafic dyke swarms in the northern of Xinjiang. *J. Earth Sci. Environ.* 36, 73–82.

Liu, B., Wu, J. H., Li, H., Mathur, R., Wu, Q. H., Zheng, H., et al. (2020). Late Paleozoic tectonic evolution of the Kangguer Shear Zone and Yamansu Arc Belt, Eastern Tianshan (NW China): constraints from structure, petrogenesis and geochronology of granitoids. *Lithos* 380–381. doi: 10.1016/j.lithos.2020.105821

Long, L. L., Wang, J. B., Wang, Y. W., Deng, X. H., Mao, Q. G., Sun, Y., et al. (2019). Metallogenic regularity and metallogenic model of the paleo arc-basin system in eastern Tianshan. *Acta Petrol. Sin.* 35, 3161–3188. doi: 10.18654/1000-0569/2019.10.13

Long, X. P., Wu, B., Sun, M., Yuan, C., Xiao, W. J., and Zuo, R. (2020). Geochronology and geochemistry of Late Carboniferous dykes in the AqishaneYamansu belt, eastern Tianshan: evidence for a post–collisional slab breakoff. *Geosci. Front.* 11, 347–362. doi: 10.1016/j.gsf.2019.06.003

Ludwig, K. R. (2003). *User's Manual for Isoplot/Ex. Version 3.00: A Geochronological Toolkit for Microsoft Excel*. Berkeley, CA: Berkeley Geochronology Center Special Publication, 1–77.

Maier, W. D., Li, C., and De Waal, S. A. (2001). Why are there no major Ni–Cu sulfide deposits in large layered mafic–ultramafic intrusions? *Can. Miner.* 39, 547–556. doi: 10.2113/gscanmin.39.2.547

Mao, J. W., Pirajno, F., Zhang, Z. H., Chai, F. M., Wu, H., Chen, S. P., et al. (2008). A review of the Cu–Ni sulfide deposits in the Chinese Tianshan and Altay orogens (Xinjiang Autonomous Region, NW China): principal characteristics and ore-forming processes. *J. Asian Earth Sci.* 32, 184–203. doi: 10.1016/j.jseaes.2007.10.006

Mao, J. W., Pirajno, F., Zhang, Z. H., Chai, F. M., Yang, J. M., Wu, H., et al. (2006a). Late Variscan Post–collisional Cu–Ni Sulfide deposits in East Tianshan and Altay in China: principal characteristics and possible relationship with mantle plume. *Acta Geol. Sin.* 80, 925–942. doi: 10.1016/S1001-8042(06)60011-0

Mao, Q. G., Xiao, W. J., Han, C. M., Sun, M., Yan, Z., Yong, Y., et al. (2006b). Zircon U–Pb age and the geochemistry of the Baishiquan mafic–ultramafic complex in the Eastern Tianshan, Xinjiang province: constraints on the closure of the Paleo–Asian Ocean. *Acta Petrol. Sin.* 22, 153–162. doi: 10.1016/j.sedgeo.2005.10.007

Mao, Y. J., Qin, K. Z., Barnes, S. J., Tang, D. M., Xue, S. C., and Vaillant, M. L. (2017). Genesis of the Huangshannan high–Ni tenor magmatic sulfide deposit in the eastern Tianshan, Northwest China: constraints from PGE geochemistry and Os–S isotopes. *Ore Geol. Rev.* 90, 591–606. doi: 10.1016/j.oregeorev.2017.05.015

Mao, Y. J., Qin, K. Z., Tang, D. M., Feng, H. Y., and Xue, S. C. (2016). Crustal contamination and sulfide immiscibility history of the Permian Huangshannan magmatic Ni–Cu sulfide deposit, East Tianshan, NW China. *J. Asian Earth Sci.* 129, 22–37. doi: 10.1016/j.jseaes.2016.07.028

Mavrogenes, J. A., and O'Neill, H. C. (1999). The relative effects of pressure, temperature and oxygen fugacity on the solubility of sulfide in mafic magmas. *Geochim. Cosmochim. Acta* 639, 1173–1180. doi: 10.1016/S0016-7037(98)00289-0

Muhtar, M. N., Wu, C. Z., Brzozowski, M. J., Li, P., Yuan, X. C., Wang, S. M., et al. (2020a). Geochronology, geochemistry, and Sr–Nd–Pb–Hf–S isotopes of the wall rocks of the Kanggur gold polymetallic deposit, Chinese North Tianshan: implications for petrogenesis and sources of ore-forming materials. *Ore Geol. Rev.* 125:103688. doi: 10.1016/j.oregeorev.2020.103688

Muhtar, M. N., Wu, C. Z., Santosh, M., Lei, R. X., Gu, L. X., Wang, S. M., et al. (2020b). Late Paleozoic tectonic transition from subduction to post-collisional extension in Eastern Tianshan, Central Asian Orogenic Belt. *Geol. Soc. Am. Bull.* 132, 1756–1774. doi: 10.1130/B35432.1

Naldrett, A. J. (1999). World–class Ni–Cu–PGE deposits: key factors in their genesis. *Miner. Deposl.* 34, 227–240. doi: 10.1007/s001260050200

Naldrett, A. J. (2010). Secular variation of magmatic sulfide deposits and their source magmas. *Econ. Geol.* 105, 669–688. doi: 10.2113/gsecongeo.105.3.669

Naldrett, A. J. (2004). *Magmatic Sulfide Deposits: Geology, Geochemistry and Exploration*. Berlin: Springer, 1–727.

Naldrett, A. J. (2009). "Fundamentals of magmatic sulfide deposits," in *New Developments in Magmatic Ni–Cu and PGE Deposits*, eds C. Li and E. M. Ripley (Beijing: Geological Publishing House), 1–26.

Ohmoto, H. (1986). "Stable isotope geochemistry of ore deposits," in *Stable isotopes in high temperature geological processes. Review in Mineralogy and Geochemistry, 16*, eds J. W. Valley, H. P. Taylor, and J. R. O'Neil (Berlin: De Gruyter), 491–559.

Pirajno, F., Mao, J. W., Zhang, Z. C., Zhang, Z. H., and Chai, F. M. (2008). The association of mafic–ultramafic intrusions and A–type magmatism in the Tianshan and Altay orogens, NW China: implications for geodynamic evolution and potential for the discovery of new ore deposits. *J. Asian Earth Sci.* 32, 165–183. doi: 10.1016/j.jseaes.2007.10.012

Qin, K. Z., Su, B. X., Sakyi, P. A., Tang, D. M., Li, X. H., Sun, H., et al. (2011). SIMS zircon U–Pb geochronology and Sr–Nd isotopes of Ni–Cu–bearing mafic–ultramafic intrusions in eastern Tianshan and Beishan in correlation with flood basalts in Tarim Basin (NW China): constraints on a ca. 280 Ma mantle plume. *Am. J. Sci.* 311, 237–260. doi: 10.2475/03.2011.03

Qin, K. Z., Tang, D. M., Su, B. X., Mao, Y. J., Xue, S. C., Tian, Y., et al. (2012). The tectonic setting, style, basic feature, relative erosion deee, ore–bearing evaluation sign, potential analysis of mineralization of Cu–Ni–bearing Permian mafic–ultramafic complexes, northern Xinjiang. *Northwest. Geol.* 45, 83–116.

Ripley, E. M., Lightfoot, P. C., Li, C., and Elswick, E. R. (2003). Sulfur isotopic studies of continental flood in the Noril'sk region: implications for the association between lavas and ore–bearing intrusions. *Geochim. Cosmochim. Acta* 67, 2805–2817. doi: 10.1016/S0016-7037(03)00102-9

Rudnick, R. L., and Gao, S. (2011). "Composition of the continental crust," in *Treatise on Geochemistry, v.3: the Crust*, ed. R. L. Rudnick (Amsterdam: Elsevier), 1–64.

San, J. Z., Qin, K. Z., Tang, Z. L., Tang, D. M., Su, B. X., Sun, H., et al. (2010). Precise zircon U–Pb age dating of two mafic–ultramafic complexes at Tulargen large Cu–Ni district and its geological implications. *Acta Petrol. Sin.* 26, 3027–3035.

Su, B. X., Qin, K. Z., Santosh, M., Sun, H., and Tang, D. M. (2013a). The Early Permian mafic–ultramafic complexes in the Beishan Terrane, NW China: alaskan–type intrusives or rift cumulates? *J. Asian Earth Sci.* 66, 175–187. doi: 10.1016/j.jseaes.2012.12.039

Su, B. X., Qin, K. Z., Tang, D. M., Sakyi, P. A., Liu, P. P., Sun, H., et al. (2013b). Late Paleozoic mafic–ultramafic intrusions in southern Central Asian Orogenic Belt (NW China): insight into magmatic Ni–Cu sulfide mineralization in orogenic setting. *Ore Geol. Rev.* 51, 57–73. doi: 10.1016/j.oregeorev.2012.11.007

Su, S. G., Tang, Z. L., Luo, Z. H., Deng, J. F., Wu, G. Y., Zhou, M. F., et al. (2014). Magmatic conduit metallogenic system. *Acta Petrol. Sin.* 30, 3120–3130.

Sun, M., Wang, Y. H., Zhang, F. F., Lin, S. Y., Xue, C. J., Liu, J. J., et al. (2020). Petrogenesis of Late Carboniferous intrusions in the Linglong area of Eastern Tianshan, NW China, and tectonic implications: Geochronological, geochemical, and zircon Hf–O isotopic constraints. *Ore Geol. Rev.* 120:103462. doi: 10.1016/j.oregeorev.2020.103462

Sun, S. S., and McDonough, W. F. (1989). "Chemical and isolopic syslematics of oceanic basalt: implications for mantle composition and processes," in *Magmatism in the Ocean Basins*, Vol. 42, eds A. D. Saunders and M. J. Norry (London: Geological Society), 313–345.

Sun, T., Qian, Z. Z., Deng, Y. F., Li, C., Song, X. Y., and Tang, Q. Y. (2013a). PGE and Isotope (Hf–Sr–Nd–Pb) constraints on the origin of the Huangshandong magmatic Ni–Cu sulfide deposit in the Central Asian Orogenic Belt, Northwestern China. *Econ. Geol.* 108, 1849–1864. doi: 10.2113/econgeo.108.8.1849

Sun, T., Qian, Z. Z., Li, C. S., Xia, M. Z., and Yang, S. H. (2013b). Petrogenesis and economic potential of the Erhongwa mafic–ultramafic intrusion in the Central Asian Orogenic Belt, NWChina: constraints from olivine chemistry, U–Pb age and Hf isotopes of zircons, and whole–rock Sr–Nd–Pb isotopes. *Lithos* 182–183, 185–199. doi: 10.1016/j.lithos.2013.10.004

Sun, T., Qian, Z. Z., Tang, Z. L., Jiang, C. Y., He, K., Sun, Y. L., et al. (2010). Zircon U–Pb chronology, platinum group element geochemistry characteristics of Hulu Cu–Ni deposit, East Xinjiang, and its geological significance. *Acta Petrol. Sin.* 26, 3339–3349.

Sun, Y., Wang, J. B., Li, Y. C., Wang, Y. W., Yu, M. J., Long, L. L., et al. (2018). Recognition of Late Ordovician Yudai porphyry Cu (Au, Mo) mineralization in the Kalatag district, Eastern Tianshan terrane, NW China: constraints from geology, geochronology, and petrology. *Ore Geol. Rev.* 100, 220–236. doi: 10.1016/j.oregeorev.2017.07.011

Sun, Y., Wang, J. B., Lv, X. P., Yu, M. J., Li, Y. C., Mao, Q. G., et al. (2019). Geochronology, petrogenesis and tectonic implications of the newly discovered Cu–Ni sulfide–mineralized Yueyawan gabbroic complex, Kalatag district, northwestern Eastern Tianshan, NW China. *Ore Geol. Rev.* 109, 598–614. doi: 10.1016/j.oregeorev.2019.05.009

Tang, D. M., Qin, K. Z., Li, C., Qi, L., Su, B. X., and Qu, W. J. (2011). Zircon dating, Hf–Sr–Nd–Os isotopes and PGE geochemistry of the Tianyu sulfide–bearing mafic–ultramafic intrusion in the Central Asian orogenic belt, NW China. *Lithos* 126, 84–98. doi: 10.1016/j.lithos.2011.06.007

Taylor, S. R., and Mclennan, S. M. (1985). *The Continental Crust: Its Composition and Evolution*. London: Blackwell Scientific Publications, 1–312.

Wang, X. S., Gao, J., Klemd, R., Jiang, T., Li, J. L., Zhang, X., et al. (2017). The Central Tianshan Block: A microcontinent with a Neoarchean–Paleoproterozoic basement in the southwestern Central Asian Orogenic Belt. *Precambrian Res.* 295, 130–150. doi: 10.1016/j.precamres.2017.03.030

Wang, Y. H., Xue, C. J., Zhang, F. F., Liu, J. J., Gao, J. B., and Qi, T. J. (2015b). SHRIMP zircon U–Pb geochronology, geochemistry and H–O–Si–S–Pb isotope systematics of the Kanggur gold deposit in Eastern Tianshan, NW China: implication for ore genesis. *Ore Geol. Rev.* 68, 1–13. doi: 10.1016/j.oregeorev.2015.01.009

Wang, Y. H., Zhang, F. F., Liu, J. J., and Que, C. Y. (2016). Genesis of the Fuxing porphyry Cu deposit in Eastern Tianshan, China: evidence from fluid inclusions and C–H–O–S–Pb isotope systemati. *Ore Geol. Rev.* 79, 46–61. doi: 10.1016/j.oregeorev.2016.04.022

Wang, Y. L., Zhang, Z. W., You, M. X., Li, X., Li, K., and Wang, B. L. (2015a). Chronological and gechemical charcateristics of the Baixintan Ni–Cu deposit in Eastern Tianshan Mountains, Xinjiang, and their implications for Ni–Cu mineralization. *Geol. China* 42, 452–467.

Wu, C. Z., Xie, S. W., Gu, L. X., Samson, I. M., Yang, T., Lei, R. X., et al. (2018). Shear zone-controlled post-magmatic ore formation in the Huangshandong Ni–Cu sulfide deposit, NW China. *Ore Geol. Rev.* 100, 545–560. doi: 10.1016/j.oregeorev.2017.02.015

Wu, H., Li, H. Q., Mo, X. H., Chen, F. W., Lu, Y. F., Mei, Y. P., et al. (2005). Age of the Baishiquan mafic-ultramafic complex, Hami, Xinjiang and its geological significance. *Acta Geol. Sin.* 79, 498–502.

Xia, L. Q., Li, X. M., Xia, Z. C., Xu, X. Y., Ma, Z. P., and Wang, L. S. (2006). Carboniferous-permian rift-related volcanism and mantle plume in the Tianshan, northwestern China. *Northwest. Geol.* 39, 1–49.

Xia, M. Z. (2009). *The Mafic-ultramafic Intrusions in the Huangshan Region Eastern Tianshan, Xinjiang: Petrogenesis and Mineralization Implication*. Doctor's thesis. Xi'an: Chang'an University.

Xia, M. Z., Jiang, C. Y., Qian, Z. Z., Xia, Z. D., Wang, B. Y., and Sun, T. (2010). Geochemistry and petrogenesis of Huangshandong intrusion, East Tianshan, Xinjiang. *Acta Petrol. Sin.* 26, 2413–2430. doi: 10.1016/j.sedgeo.2010.06.014

Xiao, B., Chen, H. Y., Hollings, P., Han, J. S., Wang, Y. F., Yang, J. T., et al. (2017). Magmatic evolution of the Tuwu–Yandong porphyry Cu belt, NW China: constraints from geochronology, geochemistry and Sr–Nd–Hf isotopes. *Gondwana Res.* 43, 74–91. doi: 10.1016/j.gr.2015.09.003

Xiao, W. J., Zhang, L. C., Qin, K. Z., Sun, S., and Li, J. L. (2004). Paleozoic accretionary and collisional tectonics of the easter Tianshan (China): implication for the continental growth of central Asia. *Am. J. Sci.* 304, 370–395. doi: 10.2475/ajs.304.4.370

Xue, S. C., Qin, K. Z., Li, C., Tang, D. M., Mao, Y. J., Qi, L., et al. (2016). Geochronological, petrological and geochemical constraints on Ni–Cu sulfide mineralization in the Poyi ultramafic–troctolitic intrusion in the NE rim of Tarim Craton, Western China. *Econ. Geol.* 111, 1465–1484. doi: 10.2113/econgeo.111.6.1465

Yang, W. Z., Ren, Y., Tian, J. T., She, J. Z., and Yang, G. G. (2017). The discovery of Lubei Cu–Ni Sulfide deposit in Eastern Tianshan, NW China and its significant. *Bull. Miner. Petrol. Geochem.* 36, 112–120. doi: 10.3969/j.issn.1007-2802.2017.01.013

Deng, Y. F., Yuan, F., Hollings, P., Song, X. Y., Zhou, T. F., Fu, B., et al. (2020). Magma generation and sulfide saturation of Permian mafic-ultramafic intrusions from the western part of the Northern Tianshan in NW China: implications for Ni-Cu mineralization. *Miner. Depos.* 55, 515–534. doi: 10.1007/s00126-019-00890-8

Zhang, J. W., Zhang, Z. W., Li, W. Y., Xie, D. S., Gao, Y. B., Wang, Y. L., et al. (2012). Chronology and geochemistry of jingbulake complex containing Cu–Ni mineralization, West Tianshan Mountain, NW China. *Northwest. Geol.* 45, 302–313. doi: 10.1007/s11783-011-0280-z

Zhang, M. J., Li, C., Fu, P. E., Hu, P. Q., and Ripley, E. M. (2011). The Permian Huangshanxi Cu–Ni deposit in western China: intrusive–extrusive association, ore genesis, and exploration implications. *Miner. Depos.* 46, 153–170. doi: 10.1007/s00126-010-0318-3

Zhang, M. J., Tang, Q. Y., Cao, C. H., Li, W. Y., Wang, H., Li, Z. P., et al. (2017). The origin of Permian Pobei ultramafic complex in the northeastern Tarim craton, western China: evidences from chemical and C–He–Ne–Ar isotopic compositions of volatiles. *Chem. Geol.* 469, 85–96. doi: 10.1016/j.chemgeo.2017.06.006

Zhang, W. F., Chen, H. Y., Peng, L. H., Zhao, L. D., Lu, W. J., Zhang, Z. J., et al. (2018). Ore genesis of the Duotoushan Fe–Cu deposit, Eastern Tianshan, NW China: constraints from ore geology, mineral geochemistry, fluid inclusion and stable isotopes. *Ore Geol. Rev.* 100, 401–421. doi: 10.1016/j.oregeorev.2017.02.021

Zhang, Z. C., Yan, S. H., Chen, B., He, L. X., He, Y. S., and Zhou, G. (2003). Geochemistry of the Kalatongke basic complex in Xinjiang and its constraints on genesis of the deposit. *Acta Petrol. Miner.* 22, 217–224.

Zhang, Z. H., Chai, F. M., Du, A. D., Zhang, Z. C., Yan, S. H., Yang, J. M., et al. (2005). Re–Os dating and ore–forming material tracing of the Karatungk Cu–Ni sulfide deposit in northern Xinjiang. *Acta Petrol. Miner.* 24, 285–293. doi: 10.1360/gs050303

Zhao, B. B., Deng, Y. F., Zhou, T. F., Yuan, F., Zhang, D. Y., Deng, G., et al. (2018). Petrogenesis of the baixintan Ni-Cu sulfide-bearing mafic-ultramafic intrusion, East Tianshan: evidence from geochronology, petrogeochemistry and Sr-Nd isotope. *Acta Petrol. Sin.* 34, 2733–2753.

Zhao, L. D., Chen, H. Y., Hollings, P., and Han, J. S. (2019). Late Paleozoic magmatism and metallogenesis in the Aqishan–Yamansu belt, Eastern Tianshan: constraints from the Bailingshan intrusive complex. *Gondwana Res.* 65, 68–85. doi: 10.1016/j.gr.2018.08.004

Zhao, L. D., Chen, H. Y., Zhang, L., Xia, X. P., Zhang, W. F., Li, D. F., et al. (2017). Geology and ore genesis of the late Paleozoic Heijianshan Fe oxide–Cu (–Au) deposit in the Eastern Tianshan, NW China. *Ore Geol. Rev.* 91, 110–132. doi: 10.1016/j.oregeorev.2017.10.014

Zhao, Y., Xue, C. J., Zhao, X. B., Yang, Y. Q., and Ke, J. J. (2015). Magmatic Cu–Ni sulfide mineralization of the Huangshannan mafic–untramafic intrusion, Eastern Tianshan, China. *J. Asian Earth Sci.* 105, 155–172. doi: 10.1016/j.jseaes.2015.03.031

Zhao, Y., Yang, Y. Q., and Ke, J. J. (2016). Origin of Cu– and Ni–bearing magma and sulfide saturation mechanism: a case study of Sr–Nd–Pb–S isotopic composition and element geochemistry on the Huangshannan magmatic Ni–Cu sulfide deposit, Xinjiang. *Acta Petrol. Sin.* 32, 2086–2098.

Zhou, M. F., Lesher, C. M., Yang, Z. X., Li, J. W., and Sun, M. (2004). Geochemistry and petrogenesis of 270 Ma Ni–Cu–(PGE) sulfide– bearing mafic intrusions in the Huangshan district, Eastern Xinjiang, Northwest China: implications for the tectonic evolution of the Central Asian orogenic belt. *Chem. Geol.* 209, 233–257. doi: 10.1016/j.chemgeo.2004.05.005

Zhou, T. F., Yuan, F., Zhang, D. Y., Fan, Y., Liu, S., Peng, M. X., et al. (2010). Geochronology, tectonic setting and mineralization of granitoids in Jueluotage area, eastern Tianshan, Xinjiang. *Acta Petrol. Sin.* 26, 478–502.

Conflict of Interest: The authors declare that the research was conducted in the absence of any commercial or financial relationships that could be construed as a potential conflict of interest.